Carbon dioxide in an ionic liquid: Structural and rotational dynamics

Chiara H. Giammanco,[a] Patrick L. Kramer,[a] Steven A. Yamada, Jun Nishida, Amr Tamimi, and Michael D. Fayer[b]
Department of Chemistry, Stanford University, Stanford, California 94305, USA

(Received 16 January 2016; accepted 16 February 2016; published online 11 March 2016)

Ionic liquids (ILs), which have widely tunable structural motifs and intermolecular interactions with solutes, have been proposed as possible carbon capture media. To inform the choice of an optimal ionic liquid system, it can be useful to understand the details of dynamics and interactions on fundamental time scales (femtoseconds to picoseconds) of dissolved gases, particularly carbon dioxide (CO_2), within the complex solvation structures present in these uniquely organized materials. The rotational and local structural fluctuation dynamics of CO_2 in the room temperature ionic liquid 1-ethyl-3-methylimidazolium bis(trifluoromethylsulfonyl)imide ($EmimNTf_2$) were investigated by using ultrafast infrared spectroscopy to interrogate the CO_2 asymmetric stretch. Polarization-selective pump probe measurements yielded the orientational correlation function of the CO_2 vibrational transition dipole. It was found that reorientation of the carbon dioxide occurs on 3 time scales: 0.91 ± 0.03, 8.3 ± 0.1, 54 ± 1 ps. The initial two are attributed to restricted wobbling motions originating from a gating of CO_2 motions by the IL cations and anions. The final (slowest) decay corresponds to complete orientational randomization. Two-dimensional infrared vibrational echo (2D IR) spectroscopy provided information on structural rearrangements, which cause spectral diffusion, through the time dependence of the 2D line shape. Analysis of the time-dependent 2D IR spectra yields the frequency-frequency correlation function (FFCF). Polarization-selective 2D IR experiments conducted on the CO_2 asymmetric stretch in the parallel- and perpendicular-pumped geometries yield significantly different FFCFs due to a phenomenon known as reorientation-induced spectral diffusion (RISD), revealing strong vector interactions with the liquid structures that evolve slowly on the (independently measured) rotation time scales. To separate the RISD contribution to the FFCF from the structural spectral diffusion contribution, the previously developed first order Stark effect RISD model is reformulated to describe the second order (quadratic) Stark effect—the first order Stark effect vanishes because CO_2 does not have a permanent dipole moment. Through this analysis, we characterize the structural fluctuations of CO_2 in the ionic liquid solvation environment, which separate into magnitude-only and combined magnitude and directional correlations of the liquid's time dependent electric field. This new methodology will enable highly incisive comparisons between CO_2 dynamics in a variety of ionic liquid systems. [http://dx.doi.org/10.1063/1.4943390]

I. INTRODUCTION

Levels of carbon dioxide in the atmosphere are quickly rising and interest is growing in technologies for mitigation, either through a reduction in production or through capture.[1] Forays into removing CO_2 directly from the atmosphere with current technology have been disappointing and fall woefully short of sufficient capacity. Thus, the solution that remains is to capture the gas before it enters the atmosphere.[2] There have been many systems proposed for the capture of carbon dioxide, including various solvents, amines, polymers, metal organic frameworks, and ionic liquids (ILs).[3,4] Current DOE cost and efficiency targets for the removal of the carbon dioxide produced from power plant emissions[5] cannot be achieved with the leading amine-based capture technology.[6] The focus then must shift to more efficient removal and the development of materials and conditions to optimize the process.

For post-combustion capture of CO_2 to be efficient, the capturing medium must be reused many times. If CO_2 is bound irreversibly, an impossibly large amount of material would be required to capture the 2.2×10^9 metric tons of carbon dioxide produced in 2013 in the US alone.[7] Thus, the capture material must be able to take out carbon dioxide from the waste gas stream selectively and in high yield, release the gas later for collection, and then be recycled. Typically, a pressure or temperature swing is employed to release the absorbed gas. Ideally, it would take as little energy as possible to recover the CO_2 and the capture medium would continue working and not degrade or evaporate over many cycles. Many molecular solvents employed to date can remove carbon dioxide effectively, but they require high pressures inaccessible in post-combustion waste gas streams and can suffer from evaporative losses.

Room temperature ionic liquids (RTILs) are salts that remain molten at or below room temperature and offer many advantages for carbon capture. As they consist of discrete cations and anions, RTILs often have incredibly

[a]C. H. Giammanco and P. L. Kramer contributed equally to this work.
[b]Author to whom correspondence should be addressed. Electronic mail: fayer@stanford.edu

low vapor pressures and so do not evaporate readily. Their chemical properties are also highly tunable, with constituent ions that are readily functionalized, and hence can be made task-specific.[8–11] Even non-optimized, at atmospheric pressures, several ionic liquids, particularly those based on the imidazolium cation, show high solubility and selectivity for CO_2.[4,12–14] Some forays have been made towards functionalizing ILs for carbon capture through the addition of amine groups that can chemically bond the carbon dioxide.[15,16] However, the thermodynamic properties of these systems have not been thoroughly explored or optimized.[17,18] To search for an optimal solvent, it is important to understand what is contributing to the carbon dioxide solvation structures and dynamics so that those properties can be tuned and exploited. 1-ethyl-3-methylimidazolium bis(trifluoromethylsulfonyl)imide (EmimNTf$_2$, see Figure 1) is a particularly well studied aprotic ionic liquid, which has a high CO_2 solubility,[12,19] low viscosity, and good thermal and electrochemical stability.[20,21] Thus, it is a good first test case for exploring the dynamics of carbon dioxide in an ionic liquid system.

Previous studies have investigated the amount of carbon dioxide various materials can hold as well as the rate of CO_2 translational diffusion through these materials.[13,22–30] One other study has looked at the dynamics of the CO_2 in ionic liquids using two-dimensional infrared (2D IR) measurements of CO_2's spectral diffusion to infer structural dynamics.[31] This paper builds upon the previous study by examining the spectral diffusion dynamics in more detail, and additionally, explores CO_2 rotational dynamics for the first time.

Extensions of the 2D IR experiments to multiple polarization configurations reveal that carbon dioxide in ionic liquids undergoes reorientation-induced spectral diffusion (RISD), a phenomenon that has recently been encountered for small molecule probes in different ionic liquid systems.[32,33]

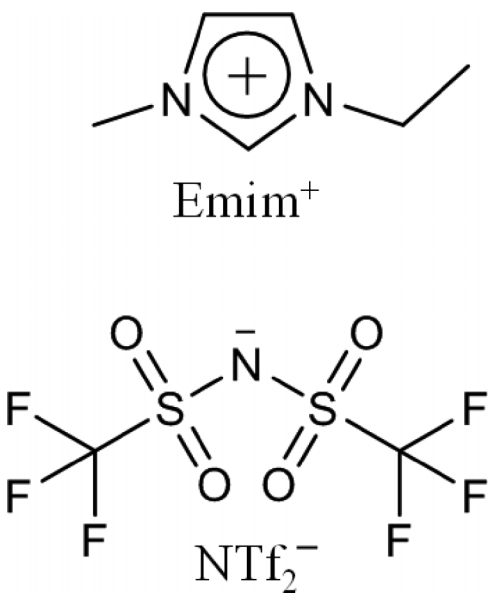

FIG. 1. Structure of the ionic liquid used: 1-ethyl-3-methylimidazolium bis(trifluoromethylsulfonyl)imide. Abbreviated to EmimNTf$_2$ throughout the paper.

RISD is the result of a vibrational probe experiencing strongly directional interactions and having fast rotational degrees of freedom, while a component of the surrounding structure evolves much more slowly. Reorientation of the probe samples this directional interaction more rapidly than the overall structural evolution of the medium does. The 2D IR measurement of the frequency-frequency correlation function (FFCF), which quantifies spectral diffusion rates and fluctuation amplitudes, is directly impacted by RISD. Different polarization configurations of the excitation pulses and emitted signal result in distinct FFCF decays because each measurement configuration samples a differently weighted ensemble of rotating molecules. Analysis of the total spectral diffusion must take this RISD contribution into account to obtain the structural spectral diffusion (SSD). Measurement and a complete analysis of the reorientation dynamics are therefore necessary for properly assigning the true structural evolution time scales and fluctuation amplitudes present in the FFCF decays.

The organization of the paper is as follows. The experimental procedures for sample preparation and an overview of the linear and nonlinear time-resolved infrared spectroscopic measurements are given in Section II. Section III contains the major results of this investigation. The linear absorption spectrum of CO_2 in the IL is presented and discussed in Section III A. The dynamics underlying this IR absorption will be extracted via the time-resolved IR techniques. Carbon dioxide's reorientation dynamics, obtained from the polarization-selective pump-probe (PP) anisotropy measurements, are analyzed in Section III B. The non-exponential decays of the orientational correlation function are assigned to a single population of solvated CO_2 molecules that undergo several periods of restricted angular diffusion (wobbling-in-a-cone)[32,34–39] prior to a freely diffusive randomization of orientational coordinates. Polarization-selective 2D IR spectral analysis, which yields the spectral diffusion dynamics of CO_2 in the ionic liquid, is presented in Section III C. Frequency evolution dynamics on a range of time scales, from sub-picosecond to hundreds of picoseconds, are evident. The FFCFs from 2D IR spectra in the parallel and perpendicular polarization geometries display clearly distinct spectral diffusion dynamics, a clear sign of RISD. For more straightforward comparison to other techniques, such as molecular dynamics (MD) simulations, we construct the isotropically averaged two-dimensional spectra and compute the FFCF, which still contains contributions from RISD. In Section IV, RISD theory is briefly reviewed with the Stark effect model for vibrational frequency coupling to an internal electric field. While the Stark model was previously developed to first order in the electric field, this first-order term vanishes for the highly symmetric CO_2 molecule, which does not have a permanent dipole moment. Thus, the equations for polarized FFCF observables are derived with the second order (quadratic) Stark effect. Armed now with an appropriate model for the SSD and RISD, the experimental FFCF results are decomposed in Section V to reveal their structural contributions, with the orientational contribution fixed by the measured pump-probe anisotropy data. Concluding remarks, with an eye towards applying

these theoretical developments and results to further explore CO_2 dynamics in various ionic liquid (or other complex material) environments, are given in Section VI. Details of the calculations for RISD theory with the second order Stark effect model, including the particular assumptions under which the results in Section IV are applicable, are provided in the Appendix.

II. EXPERIMENTAL PROCEDURES

A. Sample preparation

The RTIL 1-ethyl-3-methylimidazolium bis (trifluoromethylsulfonyl)imide ($EmimNTf_2$) was purchased from IoLiTec Ionic Liquids Technologies Inc., dried for a week under vacuum and light heating to about 60 °C, and stored in a nitrogen glove box. The water content was below 10 ppm, as determined by coulometric Karl Fischer titration. $^{13}CO_2$ (99% purity) was purchased from Icon Isotopes and used without further purification. The isotopically labeled carbon dioxide was gently bubbled through the IL in a vial with care taken to exclude atmospheric moisture. The ionic liquid with dissolved CO_2 gas was sandwiched between 3 mm CaF_2 windows, separated by a Teflon spacer. The sample cells were assembled in a dry atmosphere to prevent water uptake by the ionic liquid. Linear infrared spectra were taken with a Thermo Scientific Nicolet 6700 FT-IR spectrometer. Background spectra of the ionic liquid were taken under identical conditions and subtracted from the carbon dioxide in ionic liquid spectra to give the contribution from the $^{13}CO_2$ alone. The carbon dioxide concentration was kept sufficiently low that vibrational excitation transfer between adjacent molecules was statistically unlikely to occur. Using the extinction coefficient of carbon dioxide in water[40] and aluminosilicate glasses,[41] the concentration was estimated to be around 2500 ion pairs per carbon dioxide from the background-subtracted FTIR spectrum (Section III A).

B. Ultrafast infrared techniques

Two different experimental 2D IR setups, for which the layout and procedures have been described in detail previously,[42,43] were used to record polarization-selective 2D IR spectra and IR pump-probe measurements. Both apparatuses shared the same general layout. Briefly, a Ti:Sapphire oscillator/regenerative amplifier system, operated at 1 kHz, pumped an optical parametric amplifier (OPA) based on a BBO crystal. The output of the OPA was difference-frequency mixed in a $AgGaS_2$ crystal to create mid-IR pulses. The mid-IR beams propagated in an enclosure that was purged with air scrubbed of water and carbon dioxide to minimize absorption of the IR. Some carbon dioxide remained despite the purge, but the isotopic labeling shifted the probe absorption away from this wavelength so that the data were not distorted by atmospheric $^{12}CO_2$ absorption.

The IR light was split into two beams, a stronger pump and a weaker probe, for both the pump-probe and vibrational echo measurements. To collect pump-probe data, the pump beam polarization was rotated to 45° relative to the horizontally polarized probe using a half wave plate and polarizer and was chopped at half the laser repetition rate. The pump and probe beams are focused and crossed in an approximately 100 μm diameter spot at the sample. The relative pump-probe delay was set precisely using a mechanical delay stage. After traversing the sample, the probe polarization was resolved either parallel or perpendicular to that of the pump beam by a computer controlled rotatable polarizer. The probe polarization was projected back to horizontal following the measurement before detection. For general vibrational echo experiments, three IR pulses of the desired polarizations impinge on the sample and stimulate the emission of the vibrational echo in the phase-matched direction and with polarization(s) dictated by those of the excitation pulses. To obtain phase information, the echo was heterodyned with a fourth pulse, the local oscillator (LO). The signal (probe or echo with LO) was dispersed by a spectrograph with a 300 line/mm grating and detected on a 32 pixels, liquid nitrogen cooled, mercury-cadmium-telluride array.

The two setups used differed in the bandwidth supported (and thus minimum pulse length) and the pixel width of the detecting array. The first system[42] was employed for the pump-probe measurements. It afforded greater time resolution as it had shorter pulses (~70 fs). This system was modified with a diverging lens (f = −7.5 cm) after the spectrograph (located slightly before the exit focal plane) to further spread out the dispersed wavelengths spatially. This setup enabled the array detector, with its relatively wide pixels (0.5 mm width), to better sample the resolution supplied by the spectrograph. Spectral data were retrieved every 0.6 cm^{-1}.

The second system[43] was employed in the acquisition of the vibrational echo signal and was configured in a pump-probe geometry with a Germanium acousto-optic mid-infrared pulse shaper. Three incident pulses, the first two of which are generated collinearly by the pulse shaper, stimulated the emission of the vibrational echo in the phase-matched direction, which is collinear with the third (probe) pulse. The probe serves as the LO for optical heterodyne detection of the echo signal. Though this system did not support as great an IR bandwidth as the first (and thus did not have as short time resolution), there was significantly more power at the vibrational probe absorption wavelengths and it was outfitted with an array detector with narrower pixels (0.1 mm). The narrow pixels enabled sampling the spatially dispersed spectral data with greater resolution. A width equivalent to several pixels separates the thin detector elements. To collect the frequencies lost between pixels, the monochromator center was shifted by half the pixel-to-pixel frequency spacing. The two sets of interferogram data at 32 detection frequencies each were interlaced to yield one complete data set at 64 frequencies. The pulse shaper enables phase cycling and collection of echo interferograms in the partially rotating frame for scatter removal and rapid data acquisition. The pulse shaper additionally allows 2D IR data to be worked up without the need for phase corrections in post-processing[44,45] because the echo signal is self-heterodyned by the collinear pulse 3, which serves as the LO. This method results in no uncertainty in the relative timing of pulses that define coherence periods during which there is rapid phase evolution.[43,46,47]

III. RESULTS AND DISCUSSION

A. Linear IR spectrum

Carbon dioxide has four vibrational modes: a symmetric stretch, an asymmetric stretch, and a doubly degenerate bend. In this study, the asymmetric stretch is monitored. The peak of unlabeled carbon dioxide ($^{12}CO_2$) shifts from 2350 cm^{-1} in the gas phase to 2342 cm^{-1} when solvated by the RTIL $EmimNTf_2$. The vibrational probe used was ^{13}C-labeled CO_2 to avoid the interference of atmospheric carbon dioxide (predominantly $^{12}CO_2$) with the signal. The isotopically labeled $^{13}CO_2$ absorbs at 2277 cm^{-1} in the IL (see Figure 2). Though the unlabeled carbon dioxide is a good probe in itself,[31,48] we have chosen to use the isotopically labeled species to limit the effects of atmospheric carbon dioxide interference with the measurement and distortion of the results.

Carbon dioxide dissolves quite readily in $EmimNTf_2$.[12,19] Imidazolium-based ionic liquids typically can solubilize large quantities of the gas, comparable to or better than other common cations in terms of mole fraction dissolved.[4,13,25,49] However, the anion is more important for the solubility.[19,25] Experiments and molecular dynamics simulations show a greater affinity for and a stronger organization of the CO_2 molecules around the anion.[19] The identity of anion, and to a lesser extent the cation, can cause the center of the linear IR absorption spectrum of CO_2 to shift and broaden. The partial charges on the isolated carbon dioxide molecule are rather large, with the carbon having +0.70 of a charge and −0.35 for each oxygen,[50] and so it associates quite readily with the polar groups of the ionic liquid. There is very little volume expansion when the gas is added to the ionic liquid.[51] The anion radial distribution function changes little upon the addition of CO_2[19] suggesting that the ionic liquid structure remains relatively unperturbed by the addition of small amounts of carbon dioxide, in contrast to more typical solvents. To a first approximation, carbon dioxide occupies the spaces in the RTIL that would otherwise be vacant.[51]

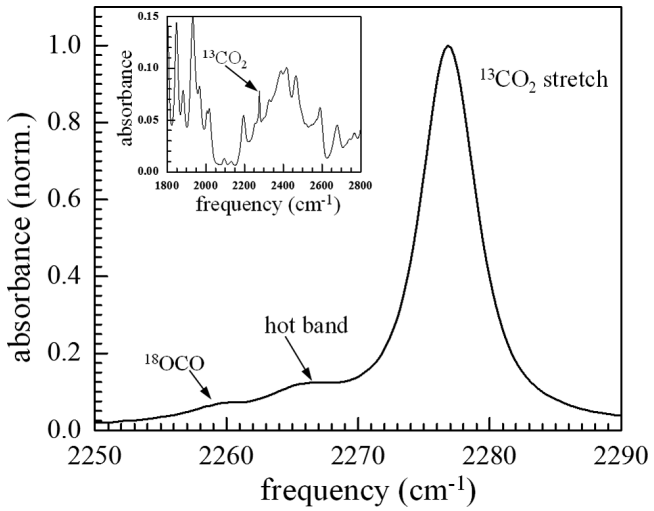

FIG. 2. Background-subtracted and normalized FTIR spectrum of $^{13}CO_2$ in the ionic liquid $EmimNTf_2$. The major shoulder on the red side is attributed to a hot band: absorption of the asymmetric stretch when the bend is already thermally excited. It is displaced to the red of the main asymmetric stretch absorption by the combination band shift. The smaller shoulder to the red of the hot band is due to a low concentration of ^{18}OCO, which accompanies the isotopically enriched $^{13}CO_2$. Inset shows the spectrum of $EmimNTf_2$ with dissolved carbon dioxide prior to subtraction of the neat IL spectrum. The location of the vibrational probe absorption is indicated on top of the IL background.

The absorption band (Figure 2) is narrow, with a 5 cm^{-1} full width at half-max (FWHM). This is somewhat narrower than the 7 cm^{-1} FWHM absorption spectrum of CO_2 in water,[48] but peak narrowing in an ionic liquid versus other solvents is not unusual.[36,52,53] The narrow band suggests either that the vibrational frequency does not change greatly as the carbon dioxide experiences different environments in the ionic liquid or that the gas molecules are found in a limited range of configurations. To the red (low frequency) side of the line there is a noticeable shoulder, both with labeled and unlabeled CO_2. It has been shown[31,54] that this shoulder is a hot band, the result of the thermally populated bend coupling to the asymmetric stretch; the absorption shows up red-shifted by the combination band shift. While the hot band does not contribute directly to the observed signal because of its redshift and low amplitude, its coupling to the fundamental transition at 2277 cm^{-1} does affect the analysis of isotropic population decay data. This topic was addressed in a previous investigation.[54] The observation of structural dynamics through spectral diffusion within the fundamental band and anisotropic reorientation dynamics is unaffected by the small isotropic population effects.[36] A very small peak further to the red is attributed to molecules that contain an ^{18}O instead of two ^{16}O. This is not unreasonable as the $^{13}CO_2$ gas is slightly enriched in ^{18}O, according to the manufacturer specifications. This peak is shifted from the main peak and has a very low amplitude. Therefore, it does not interfere with the experiments.

B. Reorientation dynamics

Polarization-selective pump-probe experiments measure both the population relaxation (vibrational lifetime) and the anisotropy (reorientation dynamics). The polarization of the pump pulse is set at 45° relative to the horizontal probe, and the polarization of the probe signal parallel ($S_{\parallel}(t)$) and perpendicular ($S_{\perp}(t)$) to the pump is then resolved. These signals can be expressed in terms of population relaxation, $P(t)$, and the second Legendre polynomial orientational correlation function, $C_2(t)$,

$$S_{\parallel}(t) = P(t)\,[1 + 0.8C_2(t)]\,, \tag{1}$$

$$S_{\perp}(t) = P(t)\,[1 - 0.4C_2(t)]\,. \tag{2}$$

The population relaxation is given by,

$$P(t) = (S_{\parallel}(t) + 2S_{\perp}(t))/3. \tag{3}$$

At early pump-probe delay times, a non-resonant signal, which tracks the pulse durations of the pump and probe interferes with the signal from the resonant vibrations. Thus, only the data after a delay time of 300 fs is used. The $^{13}CO_2$ was found to have a vibrational lifetime of 64 ± 2 ps, sufficiently long that good signal to noise data can be collected over the

longest time scales of interest for rotation and IL structural dynamics. There is also population transfer from the shoulder hot band to the main peak that occurs with the bend relaxation time. A full account of the population dynamics and the bend relaxation has been presented,[54] and so will not be reproduced here. The internal vibrational excitation dynamics present in the isotropic population decay do not interfere with the orientational relaxation measurement.[36]

The orientational relaxation of the molecules can be extracted from the anisotropy data. The pump-probe orientational anisotropy is equal to the transition dipole orientational correlation function, that is, the second Legendre polynomial correlation function, $C_2(t)$ scaled by 0.4. It has the form,

$$r(t) = \frac{S_{\parallel}(t) - S_{\perp}(t)}{S_{\parallel}(t) + 2S_{\perp}(t)} = 0.4C_2(t). \quad (4)$$

For perfect orientational correlation at time zero, the initial value is $r(0) = 0.4$. As the probe rotates, the orientational correlation function decays and the anisotropy goes to zero for complete orientational randomization. Fits of the curves do not achieve 0.4 (perfect correlation) when extrapolated back to time zero because of fast inertial motion, which occurs on ultrafast time scales within the pulse width.[55] However, by analyzing the initial deviation from 0.4, the extent of this motion can be quantified.[32,36,37,55]

The anisotropy decays of $^{13}CO_2$ in $EmimNTf_2$, at detection wavelengths spanning the entire vibrational band (see Figure 2), are presented in Figure 3. After the initial inertial drop, the curves decay in a non-exponential manner to nearly zero by 120 ps. The anisotropy data are fit well by triexponential decays. Because there is only one population

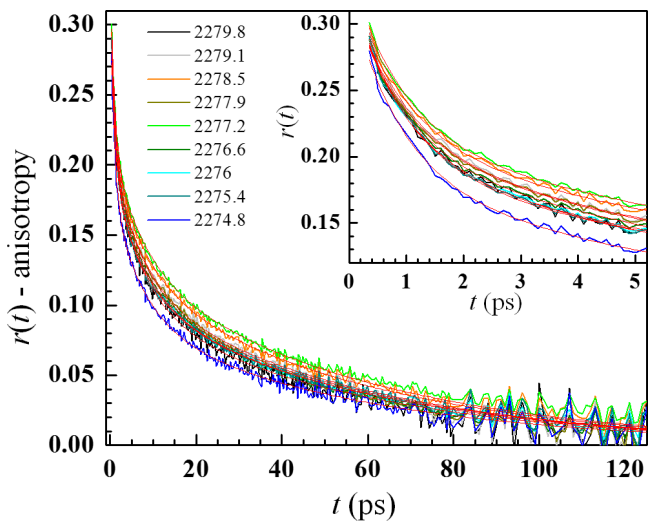

FIG. 3. Pump-probe orientational anisotropy plotted as color-coded solid lines for detection frequencies (numerical values in cm^{-1}) across the band. Triexponential decay fits to the curves are shown in red. The fits, whose time constants were shared among all frequencies but amplitudes freely varied, are in excellent agreement with the data across the entire band. The variation in the measured anisotropy with wavelength is attributed to different extents of wobbling motions (i.e., varying cone angles) across the band. The inset shows the early time data (to 5 ps) more clearly. Note that the center of the band is the highest-valued curve and the curves descend farther from the center on both sides.

of carbon dioxide molecules as was determined from the linear spectra (Figure 2) and the lifetime measurements described previously, i.e., the observed band is not made up of separate but overlapping absorption bands that result from distinct independent subensembles of molecules,[54] the anisotropy decays are interpreted as the time scales for two periods of restricted angular diffusion (wobbling-in-a-cone) and a complete rotational randomization process.[34–37] The wavelengths across the band are fit simultaneously, allowing the amplitudes of the contributing exponentials to vary while sharing the time constants. The fits, shown as the red lines in Figure 3, are in excellent agreement with the data. Allowing the long time constant to vary did not improve the quality of the fit and made the wavelengths with lower signal (at the far edges of the band) more susceptible to noise. Since the anharmonicity is so large (23 cm^{-1}) compared to the peak width, the 1-2 transition does not interfere with measurements on low frequency side of the 0-1 band. The decay time constants t_1, t_2, and t_3, which are determined self-consistently across the wavelength spread, are given in Table I.

Using the method described previously,[36,38] the cone angles are recovered from the amplitudes of the exponential terms in the anisotropy decay, and the decay time constants are associated with the correlation times of the restricted diffusive reorientation processes. The correlation time of the first cone is given simply by $\tau_{c1} = t_1$, that of the second cone is $\tau_{c2} = (1/t_2 - 1/t_3)^{-1}$, and the correlation time for the final complete orientational randomization (by free diffusion) is $\tau_m = t_3$. The inertial cone is an ultrafast motion whose complete angular range is fully sampled within the pulse duration; all we can reliably conclude about its time dependence is that it must occur with a time constant much less than about 200 fs.[55]

Each successive wobbling motion, enabled by a relaxation of constraints following structural relaxation, adds to the total angular range sampled by the probes.[36] The three cone angles, θ_{in}, θ_{c1}, and θ_{c2}, corresponding to the inertial ballistic motion, and first, and second diffusive wobbling periods, are displayed in Figure 4. The inertial cone half-angle is approximately 20° ± 2°. After the first wobbling time, the total angular range (resulting from both the inertial and first wobbling cone[38]) averaged across the band is 38° ± 2°. The total cone results from the combination of the inertial, first wobbling, and second wobbling cones and is 50° ± 2° averaged over all wavelengths. These progressively larger cones, tracking the cumulative increase in (restricted) orientational sampling by the CO_2 molecule's transition dipole, can be pulled apart into the angular contributions from each process, as if it was

TABLE I. Time constants from multi-exponential fits and wobbling-in-a-cone analysis of the orientational relaxation of small vibrational probes in $EmimNTf_2$.

Vibrational probe	$t_1 = \tau_{c1}$ (ps)	t_2 (ps)	τ_{c2} (ps)	$t_3 = \tau_m$ (ps)
$^{13}CO_2$	0.91 ± 0.03	7.2 ± 0.1	8.3 ± 0.1	54 ± 1
HOD[a]	...	4.0 ± 0.5	4.7 ± 0.7	25.1 ± 0.7
Methanol-d_4[a]	0.8 ± 0.1	5.6 ± 0.7	6.4 ± 0.9	42 ± 1
Ethanol-d_6[a]	0.8 ± 0.1	9.2 ± 0.9	10 ± 1	88 ± 10

[a]Reproduced from Kramer *et al.*[36]

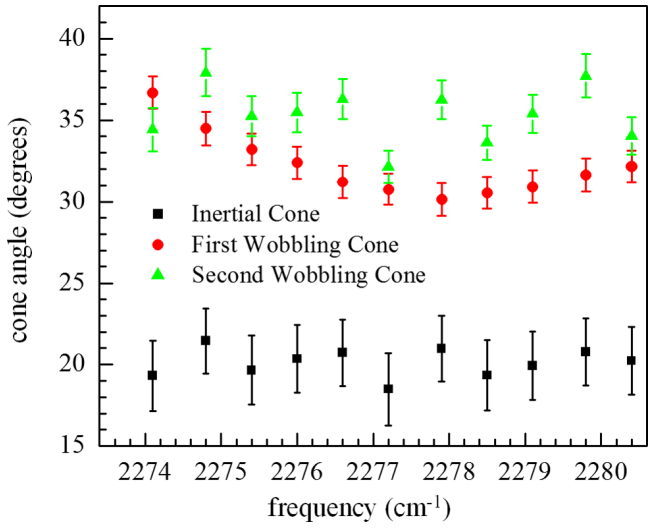

FIG. 4. Cone half angles, from the wobbling-in-a-cone analysis of the orientational anisotropy decays of the 0-1 band, plotted versus frequency. The inertial cone (black squares) and the second wobbling cone (green upward triangles) show little variation with wavelength. The first wobbling cone (red circles) is very strongly correlated with wavelength, becoming larger almost symmetrically with detuning from the center frequency (2277 cm^{-1}).

unaffected by the others.[38] These individual contributions can be compared to each other in amplitude as well at different wavelengths.[36]

As can be seen in Figure 4, only the first wobbling cone angle (red points) is significantly wavelength dependent. This wavelength dependence suggests that the specific environment around the CO_2 molecule, which determines the vibrational frequency, restricts the fastest observable motions in a particular manner. The other cones have fairly consistent size across the band and thus are not dependent on the specific environment of the carbon dioxide molecule within experimental uncertainty. These then reflect the time scales of the ionic liquid components, which gate the excursions of the CO_2 molecule.

The time scales of reorientation can be compared to the findings for water, methanol, and ethanol in $EmimNTf_2$.[36] These probes form hydrogen bonds with the IL anions,[52,53] whereas carbon dioxide does not, and so the angles of movement are correspondingly modified. However, the dynamics of reorientation occur on roughly the same time scales. This further supports the proposed mechanism that small molecule probe reorientation is being gated by the ionic liquid motions. Given that the molecular sizes and shapes are similar, the identity of the probe does not have a very major effect on the general time scales of reorientation.

The above results can also be compared to the rotational dynamics extracted from an MD simulation by Hazelbaker *et al.*[30] For the lowest CO_2 concentration in that study (which corresponds to a mole ratio of 25:1 IL ion pairs to carbon dioxide molecules), in the similar ionic liquid 1-butyl-3-methylimidazolium bis(trifluoromethylsulfonyl)imide ($BmimNTf_2$) at room temperature, the authors calculated an integrated 62 ps rotation time constant (for $C_2(t)$). This concentration of the carbon dioxide is approaching the dilute solution limit. Thus, the MD results can be compared to the experimentally determined reorientation dynamics in this study, even though the latter are from solutions that are almost 100 times more dilute. Although it is for a different ionic liquid and at a higher dissolved gas concentration, the rotational correlation time constant from the MD simulation and the experimental longest time constant of 54 ± 1 ps measured here are remarkably close.

The data can also be compared to predictions of rotational diffusion in the hydrodynamic limit, using a modified Debye-Stokes-Einstein (DSE) equation. The longest reorientation time scale, τ_m, is equal to 1/6 D_r (with D_r the diffusion constant for this final rotational process). If the diffusive motion is well described by hydrodynamics, we can relate the time scale to properties of the system by,[56]

$$\tau_m = \frac{f V_{\text{eff}} \eta}{k_B T}, \tag{5}$$

where T is temperature, η is viscosity, k_B Boltzmann's constant, and V_{eff} is the effective molecular volume. The shape factor is $f = 1$ for stick boundary conditions and $f(\rho)$ for slip conditions, where ρ is the axial ratio of the molecular ellipsoid. The ρ dependence of f with the slip boundary condition has been calculated by Youngren *et al.* and Hu *et al.*[57,58] We estimate the dimensions of the carbon dioxide molecule using the known bond length, 116 pm,[59] and the van der Waals radii of carbon and oxygen. The effective volume is then $V_{\text{eff}} = 22.4$ Å^3, $\rho = 0.58$, and $f = f(\rho) = 0.215$ for a prolate spheroid. Using our measured value $\eta = 35.8$ cp for the viscosity at 298 K, $\tau_m^{\text{stick}} = 210$ ps and $\tau_m^{\text{slip}} = 45$ ps. The stick boundary condition was originally derived for systems where a layer of much smaller solvent molecules adhere to the surface of a larger solute. As the solute rotates, the "stuck" layer of solvent is carried with it, and interactions with the surrounding solvent are responsible for friction. While the physical system studied here is not consistent with the stick model (the solute is smaller than the solvent), small solutes that have strong, specific, interactions with the solvent sometimes yield diffusion rates consistent with stick boundary conditions. Slip boundary conditions describe situations where the only friction preventing the solute from rotating freely is overlap of the swept volume of the solute with regions occupied by the solvent. Because the carbon dioxide is a small molecule located among the large ions that comprise the ionic liquid, slip boundary conditions should apply. Note that the experimentally measured 54 ± 1 ps is relatively close to the slip value of 45 ps.

If the molecular motions are truly hydrodynamic, the friction term governing both rotational and translational diffusion is the same. The rotational diffusion constant can be compared to the translational diffusion constant to determine if the system displays Stokes-Einstein (SE) behavior, i.e., is actually described well by hydrodynamics. The Stokes-Einstein-Sutherland equation gives the translational diffusion constant as,

$$D_T = \frac{k_B T}{6\pi\eta r},$$

where $r = 3/(4\pi) \times V_{\text{eff}}^{1/3}$ is the effective radius, and the other values are the same as in Eq. (5). Substituting in the numbers

from above gives $D_T = 3.5 \times 10^{-11}$ m^2/s. At room temperature and a pressure of 1 atm, the diffusion constant of carbon dioxide through EmimNTf$_2$ is 5×10^{-10} m^2/s, as measured by thin film pressure drop[23] and gravimetric[29] techniques. This is an order of magnitude faster than predicted. However, the diffusion of neutral solutes through ionic liquids is not necessarily hydrodynamic.[60] For small neutral solutes, according to Araque *et al.*,[61] the diffusion is altered by the local friction (which is not described well by the bulk IL viscosity). In this case, the SE equation is clearly violated. Thus, while the long- time scale rotational behavior can be approximated by hydrodynamics (i.e., the DSE equation with slip boundary conditions) rather well, the translational diffusion cannot.

C. Spectral diffusion

To determine the spectral diffusion dynamics of carbon dioxide in the ionic liquid, 2D IR spectroscopy experiments were performed.[44,62–64] In this third-order nonlinear time resolved technique, three excitation pulses impinge on the sample and following the third pulse give rise to the vibrational echo signal, which is an IR pulse emitted in the phase-matched direction. A fourth pulse, serving as a LO, is overlapped spatially and temporally with the signal pulse for optical heterodyne detection, which provides the requisite phase resolution and amplifies the small signal. The time delay between pulses 1 and 2 is the coherence time, τ, and the time between pulses 2 and 3 is the population time (waiting time), T_w. Data are collected by scanning τ, while fixing T_w at each desired value of the waiting time, causing the vibrational echo phase to evolve in time (τ) relative to the LO pulse. The resulting temporal interferogram is frequency resolved and detected on the 32-element array, providing the vertical axis, ω_m, of the 2D IR spectra. At each ω_m, the interferogram is numerically Fourier transformed to give the horizontal axis, ω_τ, of the 2D IR spectra.

The first and second pulses label the initial probe frequencies and create a population state. During the waiting time T_w, the structure of the liquid evolves, which causes the vibrational frequencies to shift as the particular interactions of each molecule contributing to the inhomogeneous absorption line evolve. Note that any change in the vibrational frequency of the probe (spectral diffusion) will contribute regardless of whether it is from the structural evolution of the matrix surrounding the probe or from reorientation of the probe in a quasi-static environment. The T_w period is ended by the arrival of the third pulse, which also stimulates the emission of the vibrational echo pulse. The echo contains information on the final frequencies of the vibrational oscillators.

The two dimensional spectrum then can be understood by reading off which frequencies were initially absorbed from the ω_τ axis and which frequencies were emitted on the ω_m axis. At times before spectral diffusion is complete, the 2D band shows up as elongated along the diagonal—corresponding to a vibrational oscillator only being able to sample frequencies close to its initial frequency, but not the entire inhomogeneously broadened absorption line. When correlation between the starting frequencies and ending frequencies has been lost, spectral diffusion is complete, and the peak appears symmetrically rounded. The limit of complete spectral diffusion is only experimentally accessible if the vibrational lifetime is sufficiently long compared to the slowest spectral diffusion time scale. Thus, the structural dynamics of the liquid can be extracted from the change in shape of the 2D IR spectra as a function of T_w.

The amplitudes and time scales of spectral diffusion are quantified by the FFCF. The FFCF is the joint probability that a vibrational oscillator with an initial frequency will have that same frequency at a later time, averaged over all of the initial frequencies in the inhomogeneous spectral distribution. The Center Line Slope (CLS) method[63,64] is used to extract the FFCF from the T_w-dependent shape of the 2D IR spectra. The CLS has been previously shown to be mathematically equivalent to the normalized T_w-dependent portion of the FFCF.[63,64] The complete FFCF is modeled with the form,

$$C(t) = \langle \delta\omega(t)\delta\omega(0)\rangle = \frac{\delta(t)}{T_2} + \sum_i \Delta_i^2 \exp(-t/\tau_i), \quad (6)$$

where Δ_i and τ_i are the frequency fluctuation amplitude and time constant, respectively, of the ith component. A component of the FFCF is motionally narrowed and is a source of homogeneous broadening in the absorption line shape if $\Delta_i\tau_i < 1$. In this case, it is not possible to determine Δ_i and τ_i separately. The homogeneous contribution to the FFCF is given by the first term on the right hand side of Equation (6). The homogeneous portion of the absorption spectrum has a pure dephasing linewidth given by $\Gamma^* = \Delta^2\tau/\pi = 1/(\pi T_2^*)$, where T_2^* is the pure dephasing time. The total homogeneous dephasing time that is measured, T_2, also depends on the orientational relaxation and vibrational population relaxation and is given by,

$$\frac{1}{T_2} = \frac{1}{T_2^*} + \frac{1}{2T_1} + \frac{1}{3T_{\text{or}}}, \quad (7)$$

where T_1 and T_{or} are the vibrational lifetime and orientational relaxation time. The homogeneous contribution to the line shape is a Lorentzian with FWHM $\Gamma = 1/(\pi T_2)$. The Δ_i in Eq. (6) are standard deviations of the individual Gaussian contributions to the inhomogeneous linewidth.

If the probe only experienced structural fluctuations of the surrounding fluid without undergoing independent motion (reorientation), the structural fluctuations would completely determine the FFCF. However, recent polarization-selective 2D IR experiments have shown (using an ionic liquid as the solvent) that the probe itself can rotate on a time scale fast enough that the surrounding fluid acts as a quasi-static interaction potential, such that the rotation of the probe contributes significantly to changes in its frequency, independent of fluid structural fluctuations.[32,33] This RISD contribution, when it occurs as it does here (see below) needs to be accounted for when analyzing the total FFCF to extract the rates and amplitudes of spectral diffusion processes caused by liquid structure rearrangements. The presence of RISD causes the measured spectral diffusion to proceed faster than the contribution from the structural spectral diffusion alone. If all of the spectral diffusion already occurs faster than

the rotation times including orientational wobbling, no RISD effect will be observed.

To determine if RISD is occuring, two polarization configuration vibrational echo experiments were conducted. $\langle XXXX \rangle$ and $\langle XXYY \rangle$ polarization configuration 2D IR spectra were taken, where an X indicates a beam polarized horizontally and Y is the orthogonal vertical polarization. $\langle XXYY \rangle$ means the first two pulses are vertically polarized and the third pulse and the detected echo polarization have horizontal polarization. When all frequency fluctuations are caused by liquid structure evolution, the $\langle XXXX \rangle$ 2D spectra are sufficient to quantify the spectral diffusion; in this case, the time dependence of the $\langle XXYY \rangle$ spectra will be identical to that of the $\langle XXXX \rangle$ spectra. This has been shown to be the case in bulk water, for example, from polarization-selective 2D IR experiments on the O–D stretch of dilute HOD in H_2O.[33] However, once rotation becomes significantly faster than some structural evolution time scales, the experimentally observed spectral diffusion is no longer the same for the different polarizations.

Significant RISD contributions have been observed with small molecule probes in ionic liquids, in particular, $EmimNTf_2$.[65] Therefore, measurements were taken to see if RISD occurred in the carbon dioxide–IL system. 2D infrared spectra at several waiting times in both the parallel pumped, $\langle XXXX \rangle$, and perpendicular pumped, $\langle XXYY \rangle$, configurations are displayed in Figure 5. As T_w is increased, there is a clear change in both sets of 2D band shapes from generally correlated along the diagonal (dashed lines in Figure 5) to progressively more rounded as spectral diffusion occurs over longer time intervals.

The T_w-dependent progress of spectral diffusion for both polarizations is determined quantitatively using the CLS method.[63,64] The center line slope curve is the normalized FFCF; the difference from 1 at $T_w = 0$ is determined by the homogeneous contribution to the absorption spectrum and can

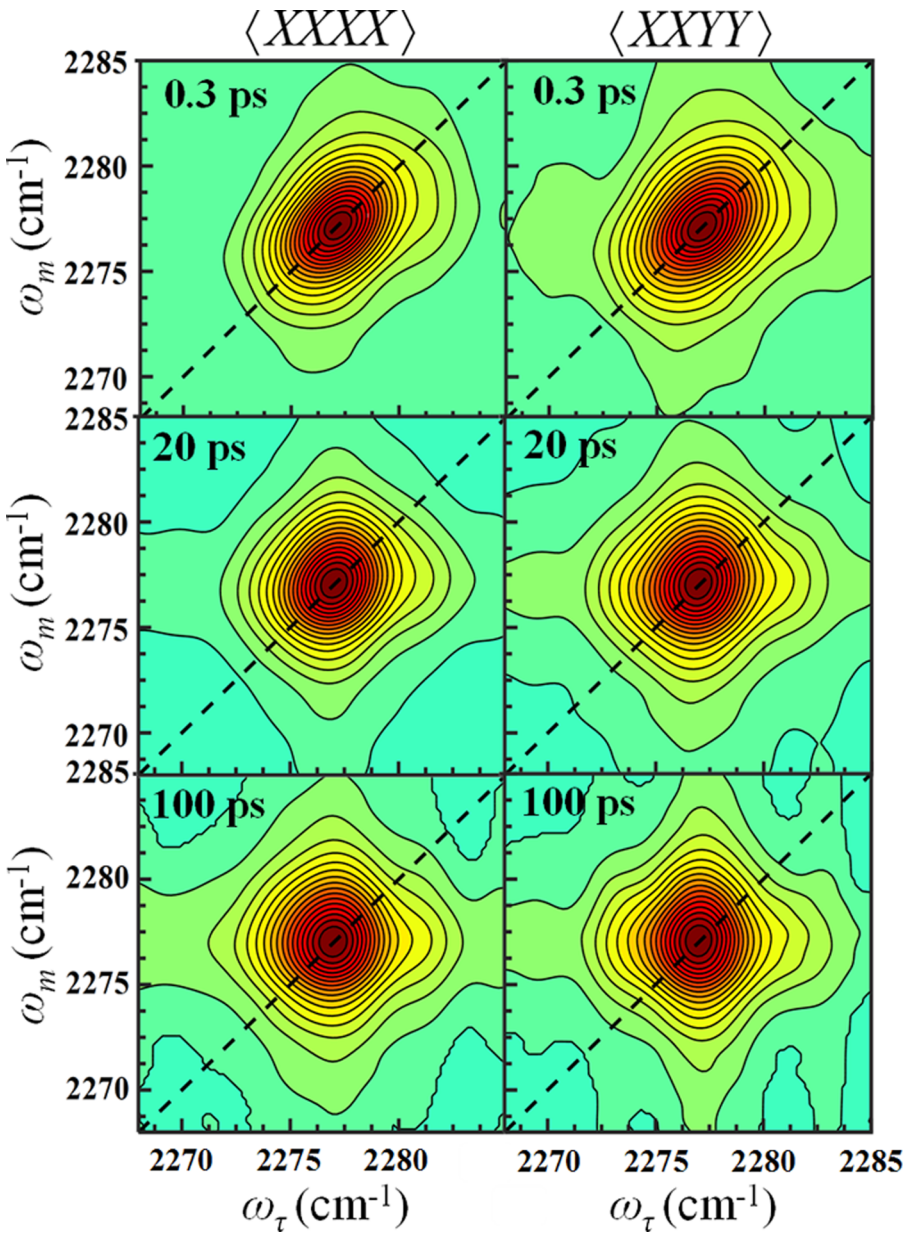

FIG. 5. 2D IR spectra of $^{13}CO_2$ in $EmimNTf_2$ for the $\langle XXXX \rangle$ (left column) and $\langle XXYY \rangle$ (right column) polarization configurations at different waiting times. Note that as the waiting time increases the spectra become more rounded and less elongated along the diagonal (black dashed line) due to spectral diffusion.

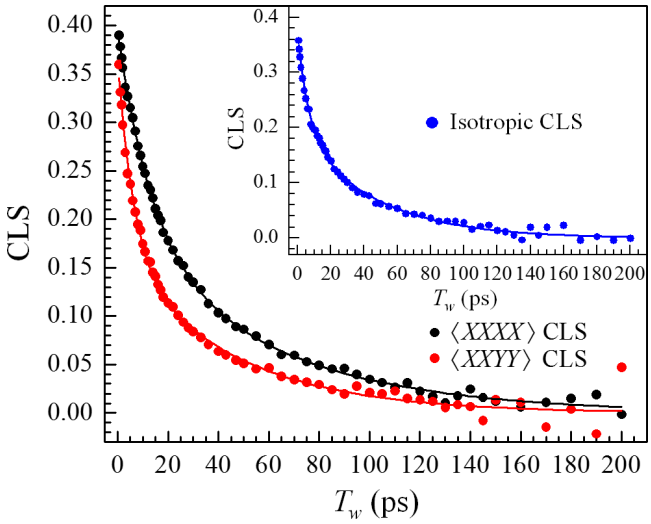

FIG. 6. Spectral diffusion of carbon dioxide's asymmetric stretch in EmimNTf$_2$, as quantified by the Center Line Slope (CLS) of 2D IR spectra taken in the $\langle XXXX\rangle$ (black dots) and $\langle XXYY\rangle$ (red dots) polarization configurations. Inset shows the CLS of the isotropic 2D spectra constructed as $\langle XXXX\rangle + 2\langle XXYY\rangle$ from the correctly normalized components (see Section III C). Solid lines are independent biexponential fits to the three decay curves (results in Table II).

be used to determine the homogeneous linewidth. The results of the CLS analysis are shown in Figure 6 (points). Loss of frequency correlation is apparent on several time scales in the normalized FFCF, with complete randomization occurring within 200 ps. Furthermore, it is clear that the $\langle XXXX\rangle$ (black dots) and $\langle XXYY\rangle$ (red dots) CLS data sets are not the same; the $\langle XXYY\rangle$ CLS data decay more rapidly with T_w than the $\langle XXXX\rangle$ data. This is precisely the trend anticipated for systems whose spectral diffusion has rotation-induced components.[32,33]

While having the $\langle XXXX\rangle$ and $\langle XXYY\rangle$ polarization configuration data will be critical to the following analysis, it is also useful to consider the isotropic 2D spectral data. The isotropically averaged spectra and corresponding FFCF are useful for comparison to MD simulations. When no laser field polarization factors are included in extracting observables from a simulation, the simulation results will still include the RISD, but the values are isotropically averaged. These data could be acquired experimentally as a separate experiment using magic angle polarization but it can also be constructed from the $\langle XXXX\rangle$ and $\langle XXYY\rangle$ data, in analogy with pump-probe $S_\parallel$ and $S_\perp$ as given in Eq. (3). To add the spectra together, they must have the correct relative amplitudes. Since the echo experiments were taken sequentially, under different laser conditions and with different polarizers, there is no guarantee that they have the same overall normalization and can be simply added together. To obtain the correct relative amplitudes, the projection of the full 2D IR spectrum onto the ω_m axis was compared to the polarization pump-probe data, $\langle XXXX\rangle$ with $S_\parallel$ and $\langle XXYY\rangle$ with $S_\perp$. The projection and PP data must be the same, up to an overall normalization factor, from the projection-slice theorem.[45] Comparing the amplitude of the projection to the pump-probe data at multiple waiting times (typically earlier T_w spectra with good signal to noise) yielded a best-fit scaling constant, which was then used to scale the entire 2D IR spectra set. Following the correct scaling of the amplitudes, the 2D spectra were linearly combined as $\langle XXXX\rangle + 2\langle XXYY\rangle$, to produce the isotropic spectrum from which the isotropic CLS curve was obtained. The isotropic curve is shown in the inset of Figure 6.

FFCF analysis was performed on the fits to the CLS of all 3 configurations and is summarized in Table II. All CLS curves fit to biexponentials. The fits are the solid curves through the data points in Figure 6. Due to the different polarization weightings of the RISD contribution, the amplitudes and time constants generated from these fits are not the same. This demonstrates how important it is to identify systems that display RISD and account for it. If only the $\langle XXXX\rangle$ configuration data had been collected (as is often done when the spectral diffusion dynamics are investigated), the time scale of the fast process would be reported as twice as slow as in the isotropic case. If these numbers are used to validate a simulation, this discrepancy could lead to erroneous conclusions. In addition, it is possible to separate the polarization dependent FFCFs shown in Figure 6 into contributions from structural spectral diffusion and rotation induced spectral diffusion, permitting the time dependence of the structural evolution of the system to be explicated. This is done below.

By separating the RISD contribution to the FFCF from the structural spectral diffusion, more can be learned about this system. A previously developed theory for calculating the polarization-selective FFCF observables, making use of a straightforward model,[32,33] suggests that the data could be fit to separate the contributions of structural spectral diffusion from the reorientation of the probe in these decays. However, applying this theory to the spectral diffusion of carbon dioxide requires care. The theory,[33] which has been successful in a previous analysis of polarization-dependent spectral diffusion data,[32] assumes that the polarization-dependence of the time-dependent 2D line shapes emerges from a polarization-dependent FFCF entering the normal nonlinear response function calculations.[66] This variable correlation function is a polarization-weighted FFCF in which the ensemble average includes weighting by the vibrational probe transition dipole's overlap with the four electric field polarization vectors involved in the excitation of the molecule and emission of the signal field.[33] The previously developed model assumed that the vibrational transition in question coupled to a quasi-static electric field, induced by the surrounding solvent, via the

TABLE II. Complete FFCF parameters that include the combined effects of structural spectral diffusion and reorientation induced spectral diffusion.

Polarization	Γ (cm^{-1})[a]	Δ_1 (cm^{-1})	τ_1 (ps)	Δ_2 (cm^{-1})	τ_2 (ps)
$\langle XXXX\rangle$	3.4 ± 0.1	0.94 ± 0.03	13.0 ± 0.7	1.11 ± 0.03	58 ± 2
$\langle XXYY\rangle$	3.6 ± 0.1	0.98 ± 0.03	6.2 ± 0.7	1.04 ± 0.03	44 ± 3
Isotropic[b]	3.5 ± 0.1	0.89 ± 0.03	6.6 ± 0.7	1.13 ± 0.03	45 ± 2

[a]$\Gamma = 1/(\pi T_2)$ is the FWHM of the Lorentzian homogeneous linewidth, with T_2 the total dephasing time. The frequency fluctuation amplitudes Δ_1 and Δ_2 are standard deviations of the Gaussian inhomogeneous line shapes, which are convolved for the total inhomogeneous contribution $\Delta^2_{\text{total}} = \Delta^2_1 + \Delta^2_2$. All three configurations give a total inhomogeneous linewidth of ~5.6 cm^{-1} (given as FWHM = $2.355 \times \Delta_{\text{total}}$).
[b]Calculated by constructing the isotropic data from the correctly normalized parallel and perpendicular 2D IR spectra and then obtaining the CLS.

first order Stark effect.[32,33] For molecules with a permanent dipole moment, the use of the first order Stark mechanism has worked well in reproducing 2D IR data in a variety of simulations.[67–74] A frequency shift due to the first order Stark effect requires the molecule to have a permanent dipole. Because carbon dioxide is a linear molecule with a reflection plane perpendicular to the axis, no such dipole is present. To quantitatively decompose the observed polarization-dependent CLS decays into their structural and rotational contributions, a new model for evaluation of the polarization-weighted FFCF observables was developed based on the *second order* (quadratic) Stark effect.

IV. RISD THEORY AND FFCF DECOMPOSITION FOR THE SECOND ORDER STARK EFFECT

A molecule in a condensed phase system can experience highly directional interactions with its surroundings, which are a major factor in determining the instantaneous vibrational frequency (frequency within the inhomogeneous absorption spectrum) of an infrared absorption mode of interest. Spectral diffusion occurs at least in part due to the time-evolution of these directional interactions with the surroundings. Fluctuations of the liquid structure will modify the directional coupling with the vibrational transition; these dynamics change the frequency and are referred to as SSD. The SSD fluctuation amplitudes and time scales give valuable information about the structural changes of the liquid or other material in which the vibrational probe is located.

The probe molecule's reorientation will modify the directional couplings, and hence vibrational frequencies (RISD), without the necessity of structural changes in the environment (assuming the environment is not considerably modified by the molecular rotation itself). The RISD process is illustrated conceptually in Figure 7 for the CO_2 molecule. As the molecule reorients, its frequency changes, but its contribution to the 2D IR vibrational echo signal decreases

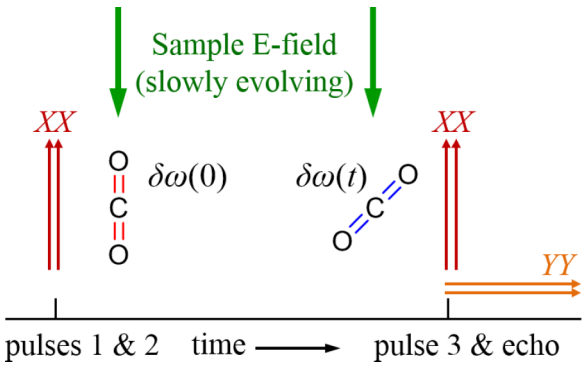

FIG. 7. Illustration of the RISD process for a linear, inversion-symmetric molecule, carbon dioxide (CO_2). The molecule experiences a relatively slowly evolving electric field that, through the second order Stark effect, is in part responsible for inhomogeneous broadening. Rotation of the molecule changes both the orientation of the transition dipole moment (parallel to the molecular axis) and the difference polarizability tensor relative to the electric field created by the environment, altering its vibrational frequency. The contribution of the frequency change to $\langle XXXX\rangle$ is reduced while the contribution to $\langle XXYY\rangle$ is increased.

in the $\langle XXXX\rangle$ case and increases for $\langle XXYY\rangle$. Our model for strongly directional interactions that can lead to RISD, and hence differences between 2D IR observables in different polarization configurations, is the Stark effect due to the net electric field induced at the position of the molecule by its surroundings.[32,33,67]

The shift of a particular molecule's vibrational transition frequency ω due to the Stark effect, expanded up to second order in the field, is,

$$\Delta\omega_E = \omega - \omega_0 = -\Delta\vec{\mu}\cdot\vec{E} - \frac{1}{2}\vec{E}\cdot\Delta\alpha\cdot\vec{E}, \tag{8}$$

where ω_0 is the natural oscillator frequency in the absence of electric fields, $\vec{E}$ is the net electric field vector at the position of the molecule, $\Delta\vec{\mu}$ is the dipole moment difference between the first excited state ($n = 1$) and ground state ($n = 0$), and $\Delta\alpha$ is the difference in polarizability tensor between the 1 and 0 states.[75–77] When vibrational excitation results in a non-zero change in dipole moment, the $\Delta\vec{\mu}$ term (first order Stark effect) is typically dominant and the weaker $\Delta\alpha$ term (second order Stark effect) can often be ignored.[76] Previous theoretical treatments of RISD in 2D IR spectroscopy, showing excellent agreement with experimental observations of hydrogen-bonded hydroxyls in an ionic liquid, have focused on the first order Stark effect's contribution to inhomogeneous broadening.[32,33] However, a molecule with inversion symmetry, e.g., carbon dioxide, cannot have a permanent dipole moment and its vibrational modes will not have difference dipoles, $\Delta\vec{\mu}$. The second order Stark effect is a conceptually straightforward model, which can lead to directional couplings of these molecules' vibrational frequencies to their environments. In particular, second order Stark shifts are naturally invariant to 180° molecular rotations, a requisite feature of any appropriate model of the frequency fluctuations for molecules (CO_2) that have such symmetry. The polarization-weighted frequency-frequency correlation functions (PW-FFCFs)[33] for the second order Stark model, which describe the polarization-selective time-dependent 2D IR band shapes as discussed in Section III C, are derived in the Appendix. The results are briefly discussed here.

Unlike first order Stark effect coupling, the second order model permits the separation of the scalar magnitude and vector direction of the field fluctuations. Rotation of a molecule will only affect the vector fluctuations, since the magnitude fluctuations are the same regardless of the probe molecule's orientation. For a particular polarization configuration, denoted p, the PW-FFCF within the second order Stark model is given in general by,

$$C_p(t) = \langle\delta\omega(t)\delta\omega(0)\rangle_p = F_s(t) + F_v(t)R_p^{(2)}(t), \tag{9}$$

where $F_s(t)$ is the correlation function of the scalar-coupled frequency fluctuations, $F_v(t)$ is the correlation function of the vector frequency fluctuations, and $R_p^{(2)}(t)$ is an RISD correlation function whose form is given below in Eqs. (12). The scalar-coupled correlation function is scaled by several constants that depend on the coupling and has the form,

$$F_s(t) = \lambda_2^2\left(\frac{1+2a_x}{3}\right)^2\left(\langle E^2(t)E^2(0)\rangle - \langle E^2\rangle^2\right). \tag{10}$$

The on-axis and off-axis components of the difference polarizability (see Eq. (A2) and discussion in the Appendix), $\Delta\alpha_z$ and $\Delta\alpha_x = \Delta\alpha_z a_x$, respectively, determine the coupling strength of the electric field to the vibrational frequency. Note that, for the CO_2 molecule, $\Delta\alpha_x$ is expected to be smaller in magnitude than $\Delta\alpha_z$, with either the same or opposite sign. The second order Stark tuning rate has been defined as $\lambda_2 = -\Delta\alpha_z/2$. Only the magnitude, $E(t)$, of the fluctuating sample electric field vector $\vec{E}(t)$ appears in Eq. (10); field orientational dynamics and molecular probe rotation do not affect the scalar part of the PW-FFCF. The scalar FFCF therefore reports on a subset of purely structural dynamics in the material.

The correlation function of vector frequency fluctuations, appearing as the second term in (9): $F_v(t)R_p^{(2)}(t)$, has been factored into the product of a structural correlation function $F_v(t)$ and an RISD correlation function $R_p^{(2)}(t)$, similarly to previous results for PW-FFCF's with a first order Stark effect model (that contain only a vector term).[32] The vector-coupled SSD correlation function is also scaled by the coupling constants and has the form,

$$F_v(t) = \frac{4\lambda_2^2(1-a_x)^2}{9} \times \left\langle E^2(t)E^2(0)D^2_{m0}(\alpha_t,\beta_t,\gamma_t)D^{2*}_{m0}(\alpha_0,\beta_0,\gamma_0)\right\rangle, \quad (11)$$

where $(\alpha_t, \beta_t, \gamma_t)$ is the orientation of the field vector at time t and $(\alpha_0, \beta_0, \gamma_0)$ is its orientation at time zero. The D^l_{mn} are Wigner rotation matrices, which are proportional to spherical harmonics when one index is zero as in Eq. (11).[78] The angle brackets $\langle\cdots\rangle$ denote an isotropic ensemble average in Eqs. (10) and (11); these correlation functions are independent of the laser field polarizations because the molecular probe orientation does not appear. Because any axis system can be chosen to perform the isotropic average, the value of m (which can be 2, 1, 0, −1, or −2) does not affect the result in (11). From the scaling constant in Eq. (11), we see that if $a_x = 1$ (equal on- and off-axis difference polarizabilities), the vector frequency fluctuations vanish and the FFCF consists of only the scalar term, (10). If this was the situation for CO_2 in EminNTf$_2$, the polarization dependence shown in Figure 6 would not occur.

The second factor in the vector FFCF term is a normalized, polarization-weighted, correlation function of the vibrational transition dipole orientation, as defined in general in Eq. (A19). The different weighting of frequency fluctuations felt by different polarization-selected ensembles of vibrational probe molecules is entirely captured by the factor $R_p^{(2)}$, with p the particular polarization configuration of interest. Observations of RISD through a difference in FFCF with polarization are enabled by the $R_p^{(2)}$ factors of the vector coupled FFCF.

The RISD factors appearing in the vector part of Eq. (9) were evaluated using the analytical methods detailed previously[33] for the three polarization configurations of interest in this work. We obtain the expressions,

$$R^{(2)}_{\text{parallel}}(t) = \frac{1}{175}\left[\frac{28 + 215C_2(t) + 72C_4(t)}{1 + 4/5C_2(t)}\right], \quad (12a)$$

for the $\langle XXXX\rangle$ configuration,

$$R^{(2)}_{\text{perpendicular}}(t) = \frac{1}{175}\left[\frac{-14 + 155C_2(t) - 36C_4(t)}{1 - 2/5C_2(t)}\right], \quad (12b)$$

for the $\langle XXYY\rangle$ configuration, and

$$R^{(2)}_{\text{isotropic}}(t) = C_2(t), \quad (12c)$$

for the overall isotropic average or magic angle configuration. In Eqs. (12), C_2 and C_4 are the orientational correlation functions of order 2 and 4, respectively, of the vibrational probe transition dipole moment.

The RISD correlation decay factors $R_p^{(2)}(t)$ as given in Eqs. (12) are displayed in Figure 8 using a free diffusion model for the orientational motion. In this case, $C_l(t) = \exp(-l(l+1)Dt)$, with D the rotational diffusion constant. The second order orientational correlation function $C_2(t)$ is 5/2 times the anisotropy decay, which is measured in polarization-selective PP experiments.[79] In the isotropically averaged case, the normalized RISD function decays as $C_2(t)$, which is exactly the same time-dependence as the observed reorientation in a PP measurement. The parallel and perpendicular cases, as displayed in Figure 8, decay somewhat more slowly and more quickly than $C_2(t)$, respectively, and notably reach offsets of +0.16 and −0.08 in the limit of infinite delay time (in the absence of structural spectral diffusion). The frequencies of the probe molecules weighed by the input/output polarizations will not completely randomize even after a long time. This offset can be qualitatively understood in the following manner. The largest frequency jump possible is obtained by rotating a molecule 90° between time 0 and time t. Assume the molecule was initially oriented parallel to the pump polarization at time zero. After the rotation, at the later time t, it contributes maximally to the $\langle XXYY\rangle$ signal, but not at all to the $\langle XXXX\rangle$ signal. Hence, the parallel configuration tends towards residual correlation at long times, while the perpendicular configuration actually yields anti-correlation.

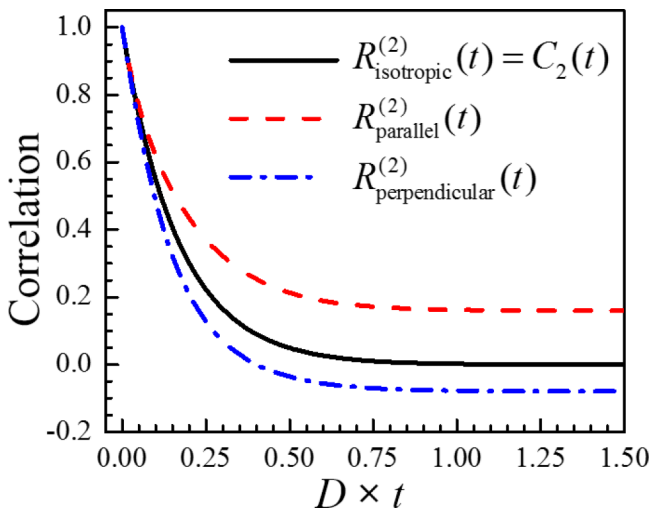

FIG. 8. The normalized, polarization-dependent parts of polarization-weighted FFCFs, in the absence of structural fluctuations. Decays are shown for the isotropic (black, solid), parallel or $\langle XXXX\rangle$ (red, dash), and perpendicular or $\langle XXYY\rangle$ (blue, dash-dot) configurations. Reorientation is assumed to be freely diffusive, with diffusion constant D. The decay in the isotropic case is simply the orientational correlation function $C_2(t)$, which is obtained directly from the pump-probe anisotropy.

On the other hand, the isotropically averaged result $C_2(t)$, which lies between these two extreme cases, decays to zero at long times.

As is evident from the form of Eq. (9), rotation of the molecule creates a distinction between structural fluctuations that only modify the square of the field magnitude, and those that cause fluctuations of both field magnitude squared and direction. While the presence of both a polarization-independent scalar term and polarization-dependent vector contribution in Eq. (9) extends the nature of the analysis of experimental 2D IR data, reorientation-induced spectral diffusion actually grants an opportunity to learn more detailed information about the fluctuations of the medium when the vibrational probe has second order Stark coupling to its surroundings. In contrast, systems with first order Stark effect coupling contain only a polarization-dependent vector term in the PW-FFCFs and therefore enable the determination of only a single structural correlation function.[32]

To confirm the presence of vector coupling between the molecular transition and the internal electric fields, 2D IR spectra should be collected and the line shapes analyzed for at least two different polarization configurations, such as $\langle XXXX\rangle$ and $\langle XXYY\rangle$ (as was done for $^{13}CO_2$ in EmimNTf$_2$ in the present investigation). Assuming the form Eq. (9) for the FFCF, F_s and F_v are the same for each polarization of the observable (e.g., CLS). Measurement of the second order orientational correlation function $C_2(t)$ in a polarization-selective PP experiment is sufficient to completely determine the $R_p^{(2)}(t)$ factor for each polarization configuration of the 2D IR data using Eqs. (12), once $C_4(t)$ is calculated from $C_2(t)$ as discussed below.[32,33] For the isotropic case, the PP measured $C_2(t)$ is the RISD function necessary in Eqs. (9) with (12c).

Constructing the $l = 4$ orientational correlation function, $C_4(t)$, from a fit to the experimentally measured $l = 2$ correlation decay requires a model. The mathematical techniques for relating orientational correlation functions of different order have been discussed in detail.[32] For free diffusion (i.e., a single exponential $C_2(t)$ decay), the transformation is straightforward; all orientational correlation functions are the single exponential forms $C_l(t) = \exp(-l(l+1)Dt)$. Multiple exponential anisotropy decays, for a single ensemble of reorienting molecules (transition dipoles), are commonly analyzed within the wobbling-in-a-cone model (see Section III B).[32,34–37,39] A fit to the pump-probe anisotropy decay (or $l = 2$ orientational correlation function) is decomposed into the product of several wobbling correlation functions: single exponential decays to a plateau (square of the generalized order parameter). These are followed by a free diffusion final reorientation factor, which is slower than all the wobbling components. The order parameter gives the hard-cone wobbling half angle θ_0. The decay time constant, $\tau_{\text{eff}}^{(l)}$, together with the cone angle allow determination of the rotational diffusion constant D_w for each wobbling regime.[36–38] The equations relating the order parameter and wobbling time constant to the cone angle and diffusion constant for $C_4(t)$ have been presented recently.[32] Each wobbling and free diffusion correlation function factor in $C_2(t)$ is transformed into the equivalent $l = 4$ correlation function, and the total $C_4(t)$ is the product of these individual factors.

V. RISD ANALYSIS FOR CO_2 IN EmimNTF$_2$

Figure 9 displays the CLS data (points, same as Fig. 6) from the $\langle XXXX\rangle$ and $\langle XXYY\rangle$ vibrational echoes as well as fits to these data (solid curves). The fits use our RISD model result, Eq. (9), with the $R_p^{(2)}(t)$ supplied by Eq. (12a) for $\langle XXXX\rangle$ or (12b) for $\langle XXYY\rangle$. Time parameters and cone angles from the anisotropy curves, $C_2(t)$, (Section III B) and the expressions for $C_4(t)$ given previously[32] in terms of the measured $C_2(t)$ were used to construct the polarization-dependent RISD factors as discussed in Section IV. While the scalar and vector components of the structural FFCF are given in Eqs. (10) and (11), neither the initial magnitudes of the scalar and vector electric field correlations nor the Stark coupling constants (λ_2 and a_x) are known *a priori*, as discussed further in the Appendix. The complete scaling prefactors in Eqs. (10) and (11) can be useful if some of these values are known through independent measurements or theoretical calculations. Therefore, the SSD correlation functions, $F_s(t)$ and $F_v(t)$, are modeled as independent multiexponentials. The RISD factors are known, and it is important to note that there are no adjustable parameters in these terms given Eqs. (12a) and (12b). The two curves shown in Figure 9 are fit simultaneously. The values of the parameters in the multiexponential functions for the scalar and vector SSD correlation functions used to fit the (normalized) FFCF data are freely varied. In the simultaneous fit, $F_s(t)$ and $F_v(t)$ are the same for the parallel and perpendicular data sets.

Trying various multiexponential forms for the scalar and vector SSD fitting function, the best results were obtained with the scalar SSD, F_s, modeled with a biexponential and the vector SSD, F_v, as a single exponential. This is the minimum number of exponentials necessary for the fit to completely describe the data. Adding more exponentials to these functions does not yield additional unique time constants

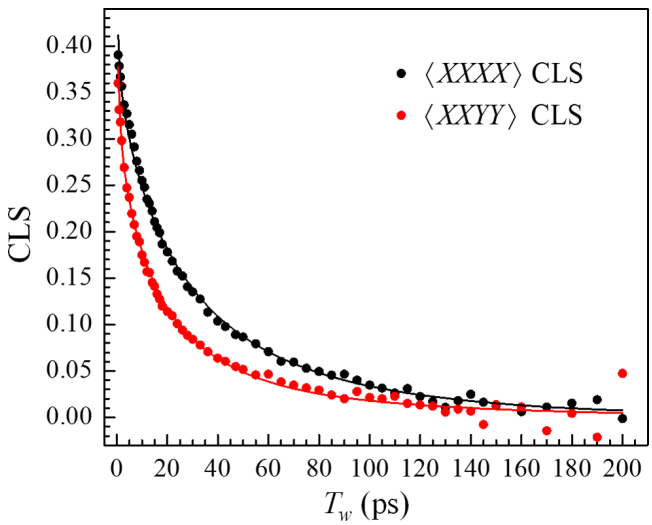

FIG. 9. CLS data points for the $\langle XXXX\rangle$ and $\langle XXYY\rangle$ 2D IR polarization configurations (same as Fig. 6 data) with the simultaneous fit to both data sets (solid lines), incorporating reorientation-induced spectral diffusion (RISD) from coupling of the vibrational transition to the solvent electric field via the second order Stark effect. The RISD terms (see Eq. (9) with Eqs. (12a) and (12b)), have no adjustable parameters. The fits determine the time dependence of the structural fluctuations.

TABLE III. Amplitudes (A_i) and time constants (τ_i) from the fit of the polarization-weighted normalized FFCFs with Eq. (9). The results are the effect of structural spectral diffusion with the contributions from reorientation induced spectral diffusion removed.

SSD Correlation function	A_1	τ_1 (ps)	A_2	τ_2 (ps)
F_s (scalar)	0.09 ± 0.02	20 ± 5	0.07 ± 0.02	77 ± 18
F_v (vector)	0.36 ± 0.01	57 ± 5	...	...

or a substantially better fit, which demonstrates that the functions chosen for F_s and F_v are sufficient, and adding more free variables over parameterizes the fit. As can be seen in Figure 9, the fits to both polarization data sets are very good. A single set of parameters for F_s and F_v yields fits to both curves. It is important to note again that $R_p^{(2)}(t)$ in Equations (9) and (12) are completely determined by the separate pump-probe anisotropy measurements. There are no adjustable parameters in $R_p^{(2)}(t)$. The fit parameters are given in Table III.

Let us now examine the time scales of the structural spectral diffusion that are obtained from the fits that separate the SSD from the RISD. The scalar part of the correlation function is composed of two exponentials with decay time constants of 20 ± 5 ps and 77 ± 18 ps. These processes contribute nearly equally to the total scalar amplitude. The vector process has a time constant of 57 ± 5 ps and is responsible for roughly two thirds of the total structural spectral diffusion. The long time constants for the two correlation functions are similar, and in fact, the error bars overlap. Therefore, it is possible that both contributions result from the same IL motions. The same fluctuation can alter both the magnitude and direction of the solvent's internal electric field at the CO_2 position. If the times are not identical, that is not surprising. The scalar and vector SSD factors are different correlation functions. Even if they report on the same dynamical process, the resulting correlation time need not be identical.

The shorter 20 ps time constant is unique, having no corresponding component in the vector fluctuations. One way this could emerge is if the frequency shifts from a class of field magnitude fluctuations are exactly counteracted by (necessarily correlated) field direction fluctuations. The scalar part, reporting only on magnitude fluctuations, would decay, but the vector part could show far less frequency decorrelation to the point that this motion is not observable as a distinct spectral diffusion time scale. Another possibility is that the additional time scale is caused by a process whose effect on the vibrational frequencies is unrelated to the Stark effect (or directional interactions in general). Non-vector structural fluctuations that induce frequency fluctuations are indistinguishable from the second order Stark contribution to the scalar SSD correlation function (see the Appendix). It is possible that the shorter dynamic time scale of 20 ps is reporting on isotropic dynamics, perhaps related to density fluctuations in the liquid,[80] that are not directional in their coupling to the vibrational transition.

These SSD numbers can also be compared to the isotropic FFCF parameters discussed above and summarized in Table II. Recall that the RISD contribution was not separated from this data; the isotropic FFCF decays on a faster time scale than the structural correlation functions alone. The fast time constant of 6.6 ps in the isotropic data is significantly faster than the actual fastest structural spectral time scale of 20 ps. This serves as a further evidence that RISD must be accounted for to correctly determine the time scales of structural fluctuations. Given that the scalar and vector components can be separated and the time scales of these motions determined, it will be important to use this analysis when comparing different experimental systems and conditions to assess which motions are affected. The vector and scalar SSD correlation functions, Eqs. (11) and (10), are quantities that could be computed directly from MD trajectories (up to scale factors for the Stark coupling strengths), which may allow precise assignment of the molecular motions contributing to the various experimentally determined time scales and fluctuation amplitudes.

One of the assumptions that is part of the RISD analysis is that the orientational relaxation of the small probe molecule itself does not modify its surroundings, causing structural spectral diffusion. This is a reasonable assumption given the size of CO_2 relative to $Emim^+$ and NTf_2^-, but there is also some experimental evidence that supports this assumption. The wobbling-in-a-cone orientational relaxation time constants (see Table I) are much faster than the fastest component of the structural spectral diffusion (see Table III). If these orientational motions induced changes in the structure of the surrounding IL, then there would be faster components in the SSD than are observed. Such fast SSD dynamics would not have identical time constants as the wobbling time constants as these are two distinct correlation functions, but the lack of fast SSD dynamics is consistent with CO_2 reorientation not inducing extensive structural changes in the surrounding IL.

Optical heterodyne detected optical Kerr effect (OHD-OKE)[81] measurements were used to measure the bulk orientational relaxation time of $EmimNTf_2$. The time constant for complete orientational randomization of the liquid is 380 ps, which is much longer than the slowest component of the SSD, 77 ps. This comparison shows that it is not necessary to entirely randomize the bulk liquid structure to have complete spectral diffusion, that is, to completely sample all structures that give rise to the frequencies in the inhomogeneously broadened absorption line. Thus, the IL structures relevant in determining a particular CO_2 molecule's solvation environment may not depend on the bulk liquid's global structure.

VI. CONCLUDING REMARKS

Here, we have described the dynamics of carbon dioxide in $EmimNTf_2$, a promising room temperature ionic liquid solvent for carbon capture. Reorientation is found to occur on 3 time scales corresponding to two different wobbling motions with time constants of 0.91 ± 0.03 and 8.3 ± 0.1 and a long time complete reorientation time constant of 54 ± 1 ps.

The spectral diffusion of the carbon dioxide has been partitioned into its structural and rotational dynamic contributions using RISD analysis. Since the molecule is inversion-symmetric and hence has no permanent dipole

moment, the previously existing RISD theory (first order Stark effect) could not be used to describe the observed behavior. In fact, attempts to fit the CO_2 data with the first order Stark effect RISD theory gave poor results. New equations were developed utilizing a second order Stark effect model for the molecular interactions with the sample electric field. The second order Stark effect provides the unique opportunity to distinguish contributions to spectral diffusion from liquid structural reorganization processes that are scalar-coupled and vector-coupled. The experiments presented here revealed the reorientation and structural fluctuations of a carbon dioxide probe in the ionic liquid $EmimNTf_2$ and lay out the methods and equations for analyzing similar systems. Future work will elucidate changes at different temperatures, chain lengths, and cations and in other ionic liquid families entirely, using these dynamics as a benchmark. The highly detailed dynamical information that these analysis methods extract from CO_2 in IL systems will provide very precise comparisons and may lead to structure-dynamics-function relationships useful for developing applications.

ACKNOWLEDGMENTS

This work was funded by the Division of Chemical Sciences, Geosciences, and Biosciences, Office of Basic Energy Sciences of the U.S. Department of Energy through Grant No. DE-FG03-84ER13251 (C.H.G., P.L.K., M.D.F., and the shorter pulse ultrafast IR spectrometer.) This material is also based upon work supported by the Air Force Office of Scientific Research (AFOSR) under AFOSR Grant No. FA9550-16-1-0104 (S.A.Y., J.N., A.T., M.D.F., and pulse shaping ultrafast IR spectrometer). P.L.K., J.N., and A.T. acknowledge support from Stanford Graduate Fellowships.

APPENDIX: EVALUATION OF SECOND-ORDER STARK EFFECT FFCF EXPRESSIONS

The time-dependent frequency shift caused by the second order Stark effect is written as,

$$\Delta\omega_E(t) = -\frac{1}{2}\vec{E}(t)\cdot\Delta\alpha(t)\cdot\vec{E}(t), \tag{A1}$$

where the net electric field and difference polarizability are both time-dependent because they are expressed in the lab frame (in which the polarizations of the four laser fields involved in a 2D IR experiment are fixed). Two additional coordinate systems will be useful in this work, the molecular frame and the sample field frame. The difference polarizability is best expressed in the molecular frame (x, y, z), where it is a time-independent diagonal rank 2 tensor,

$$\Delta\alpha = \begin{bmatrix} \Delta\alpha_x & & \\ & \Delta\alpha_y & \\ & & \Delta\alpha_z \end{bmatrix} = \Delta\alpha_z \begin{bmatrix} a_x & & \\ & a_y & \\ & & 1 \end{bmatrix} \equiv \Delta\alpha_z\Delta\mathbf{A}. \tag{A2}$$

We consider the z-axis to be the molecule's major axis (along the vibrational displacement coordinate) and focus on the normalized polarizability difference tensor $\Delta\mathbf{A}$, chosen because we anticipate $\Delta\alpha_z$ to be the major contributor. The remaining terms are $a_x = \Delta\alpha_x/\Delta\alpha_z$ and $a_y = \Delta\alpha_y/\Delta\alpha_z$.

In the lab frame, the fluctuating electric field vector is $\vec{E}(t) = E(t)\hat{e}(t)$, with E the field magnitude and $\hat{e}$ the unit vector specifying its direction. Both of these will evolve in a generally correlated manner due to the molecular motions in the medium in which the vibrational probe is embedded. We choose to begin our calculation of the observables using the sample field frame (X_F, Y_F, Z_F), which is defined such that $\hat{e}(t) = \hat{k}_F$, the unit vector along the Z_F axis. The field frame considers the time-varying electric field to have a magnitude $E(t)$ directed along the Z_F axis. Let the Euler angles $(\phi_F(t), \theta_F(t), \chi_F(t))$ specify the orientation of the molecular frame relative to the field frame at the time t. With $\Phi(\phi, \theta, \chi)$ the direction cosine matrix and $\Phi^{-1}(\phi, \theta, \chi)$ its inverse (transpose),[78] the difference polarizability in the field frame is,

$$\Delta\alpha(t) = \Delta\alpha_z\left[\Phi\left(\phi_F(t), \theta_F(t), \chi_F(t)\right)\right] \times \Delta\mathbf{A}\left[\Phi^{-1}\left(\phi_F(t), \theta_F(t), \chi_F(t)\right)\right]. \tag{A3}$$

The virtue of the field frame is that the (generally complicated) scalar product between the $\Delta\alpha(t)$ tensor and the $\vec{E}(t)$ vectors appearing in Eq. (A1) reduces to a relatively simple form with only 3 terms,

$$\begin{aligned}\Delta\omega_E(t) &= -\frac{1}{2}E^2(t)\hat{k}_F\cdot\Delta\alpha(t)\cdot\hat{k}_F \\ &= -\frac{\Delta\alpha_z}{2}E^2(t)\big(\cos^2(\theta_F(t)) + a_x\sin^2(\theta_F(t))\cos^2(\phi_F(t)) \\ &\quad + a_y\sin^2(\theta_F(t))\sin^2(\phi_F(t))\big).\end{aligned} \tag{A4}$$

The frequency shift can be cast in its most useful mathematical form by making use of the spherical harmonics Y_l^m, assuming the standard conventions.[78] Define $\Omega_F = (\theta_F, \phi_F)$ as a shorthand for the first two molecular frame to field frame transformation angles, which uniquely specify the orientation of the molecular z-axis in the sample field frame. It is straightforward to show that,

$$\begin{aligned}\cos^2(\theta_F) &= 1/3 + 4/3\sqrt{\pi/5}Y_2^0(\Omega_F), \\ \sin^2(\theta_F)\cos^2(\phi_F) &= 1/3 - 2/3\sqrt{\pi/5}Y_2^0(\Omega_F) \\ &\quad + \sqrt{2\pi/15}\left(Y_2^2(\Omega_F) + Y_2^{-2}(\Omega_F)\right)\end{aligned}$$

and

$$\begin{aligned}\sin^2(\theta_F)\sin^2(\phi_F) &= 1/3 - 2/3\sqrt{\pi/5}Y_2^0(\Omega_F) \\ &\quad - \sqrt{2\pi/15}\left(Y_2^2(\Omega_F) + Y_2^{-2}(\Omega_F)\right).\end{aligned}$$

Finally, defining an effective second order Stark tuning rate $\lambda_2 = -\Delta\alpha_z/2$, we have,

$$\Delta\omega_E(t) = \lambda_2 E^2(t)\left(\frac{1+a_x+a_y}{3} + \left(1-\frac{a_x+a_y}{2}\right) \times \frac{4}{3}\sqrt{\frac{\pi}{5}}Y_2^0(\Omega_F(t))\right) + \lambda_2 E^2(t)(a_x - a_y) \times \sqrt{\frac{2\pi}{15}}\left(Y_2^2(\Omega_F(t)) + Y_2^{-2}(\Omega_F(t))\right). \quad \text{(A5)}$$

The time-dependent second order Stark shift in Eq. (A5) can evolve due to changes in the field magnitude E and in the orientation between field and molecular frames, Ω_F. Furthermore, both changes in direction of the electric field vector $\hat{e}$ and reorientation of the molecule's z-axis cause changes in Ω_F. The latter dynamics are responsible for reorientation-induced spectral diffusion, while the field magnitude and direction changes are the sources of structural spectral diffusion within the present model.

While the treatment has been quite general so far, we can gain some additional simplification of the Stark shift functional form with the approximation, $a_x = a_y$. The focus of this work is on the vibrations of CO_2, a linear molecule, for which $a_x = a_y$ clearly holds in Eq. (A2). Even in somewhat more complex molecules this can be a reasonable approximation.[82] For these cases,

$$\Delta\omega_E(t) = \lambda_2 E^2(t)\left(\frac{1+2a_x}{3} + (1-a_x)\frac{4}{3}\sqrt{\frac{\pi}{5}}Y_2^0(\Omega_F(t))\right). \quad \text{(A6)}$$

The final term of Eq. (A5) has been eliminated and the number of parameters reduced.

The relevant ensemble averages for the PW-FFCFs were performed in the lab frame. Therefore, our final expression for the second order Stark frequency shift was written in this frame. We proceed in a similar manner to the previous treatment of the first order Stark case.[32,33] Suppose the Euler angles which transform the sample field frame into the lab frame at time t are $(\alpha_1, \beta_1, \gamma_1)$ and that the orientation of the molecular frame's z-axis in the lab frame at the same time is Ω_1. Then, using the Wigner rotation matrices D^l_{mn},[78] Eq. (A6) is transformed to,

$$\Delta\omega_E(t) = \lambda_2 E^2(t)\left(\frac{1+2a_x}{3} + (1-a_x)\frac{4}{3}\sqrt{\frac{\pi}{5}} \times \sum_m D^2_{m0}(\alpha_1,\beta_1,\gamma_1)Y_2^m(\Omega_1)\right). \quad \text{(A7)}$$

As shown in (A7), the vibrational frequency of the probe for a given electric field magnitude is uniquely determined by (1) how the probe is oriented in the lab frame (Ω_1) and (2) how the field surrounding the probe is oriented in the lab frame $(\alpha_1, \beta_1, \gamma_1)$. These two orientations determine the relative orientation between the probe and the field as appears in the second order Stark shift (A1), which is the sole source of spectral diffusion in the present model. Both of these orientations need to sample all angles in the isotropic ensemble averaging when the PW-FFCFs are calculated below.

Because the expectation value of spherical harmonics vanishes for angular momentum $l > 0$, the average of the second order Stark shift in (A7) is,

$$\langle\Delta\omega_E(t)\rangle = \lambda_2\frac{1+2a_x}{3}\langle E^2\rangle. \quad \text{(A8)}$$

The transition has a net frequency shift (to new center ω_0^E) because of the sample generated field in addition to time-dependent fluctuations with zero average. Hence, we can write the frequency fluctuation as,

$$\delta\omega(t) = \omega(t) - \omega_0^E = \Delta\omega_E(t) - \langle\Delta\omega_E(t)\rangle = \lambda_2\frac{1+2a_x}{3}\left(E^2(t) - \langle E^2\rangle\right) + \lambda_2 E^2(t)(1-a_x) \times \frac{4}{3}\sqrt{\frac{\pi}{5}}\sum_m D^2_{m0}(\alpha_1,\beta_1,\gamma_1)Y_2^m(\Omega_1), \quad \text{(A9)}$$

which satisfies the standard requirement $\langle\delta\omega(t)\rangle = 0$. Note that the frequency fluctuation contains two terms: one that depends only on the time-varying electric field magnitude squared and one that additionally depends on both the field frame and molecular frame orientations. Both terms depend on $E^2(t)$. The first term is indistinguishable from scalar sources of frequency fluctuations, e.g., due to density fluctuations that are not caused by the Stark effect.[32,80] For the second, "vector" term, the sample generated electric field orientation enters through the rotation matrices D^2_{m0}, while the molecular probe orientation affects the spherical harmonics Y_2^m. Analogous to Eq. (A9), at time $t = 0$, we assume the field frame has orientation $(\alpha_0, \beta_0, \gamma_0)$ and the molecular frame has orientation Ω_0, relative to the lab frame.

In calculating the required frequency time correlation functions, we will use the notation $\langle\cdots\rangle_p$ to represent a polarization-weighted ensemble average, where the p-polarization configuration weighting factors are the same as those used for the theory of RISD with the first order Stark effect.[33] Averages that do not depend on the molecular axis orientations Ω_0 or Ω_1 reduce to ordinary isotropic ensemble averages, written as $\langle\cdots\rangle$. Two important assumptions are necessary for evaluation of the PW-FFCFs for second order Stark coupling. First, we assume the vibrational transition dipole moment is parallel to the molecular z-axis, which contains the major contribution to the difference polarizability. For the asymmetric stretching mode of carbon dioxide this is clearly true. Therefore, the molecular frame orientation Ω_1 (or Ω_0) in Eq. (A9) is also the transition dipole orientation, which enters the polarization-dependent weighting factors.[33] Second, the sample's electric field magnitude and direction will be taken to be statistically independent of the vibrational probe's orientational coordinates, which should be applicable for a small molecule reorienting in a slowly evolving electric field with contributions from many surrounding molecules or molecular ions.[67,83] The reorientation does not necessarily occur by free diffusion, and we will not explicitly consider any net alignment of the vibrational probe with the field.

We calculate the polarization-weighted FFCF as follows. First, we write,

$$
\begin{aligned}
C_p(t) &= \langle \delta\omega(t)\delta\omega(0)\rangle_p \\
&= \lambda_2^2\left(\frac{1+2a_x}{3}\right)^2 \left\langle (E^2(t)-\langle E^2\rangle)(E^2(0)-\langle E^2\rangle)\right\rangle_p \\
&\quad + \lambda_2^2(1-a_x)^2\frac{16\pi}{45}\left\langle E^2(t)E^2(0)\sum_{m,n} D^2_{m0}(\alpha_1,\beta_1,\gamma_1)D^2_{n0}(\alpha_0,\beta_0,\gamma_0)Y_2^m(\Omega_1)Y_2^n(\Omega_0)\right\rangle_p \\
&\quad + 2\lambda_2^2\frac{(1+2a_x)(1-a_x)}{3}\frac{4}{3}\sqrt{\frac{\pi}{5}}\left\langle E^2(t)\left(E^2(0)-\langle E^2\rangle\right)\sum_m D^2_{m0}(\alpha_1,\beta_1,\gamma_1)Y_2^m(\Omega_1)\right\rangle_p \\
&= \lambda_2^2\left(\frac{1+2a_x}{3}\right)^2 \left(\left\langle E^2(t)E^2(0)\right\rangle - \langle E^2\rangle^2\right) \\
&\quad + \lambda_2^2(1-a_x)^2\frac{16\pi}{45}\sum_{m,n}\left\langle E^2(t)E^2(0)D^2_{m0}(\alpha_1,\beta_1,\gamma_1)D^2_{n0}(\alpha_0,\beta_0,\gamma_0)\right\rangle\left\langle Y_2^m(\Omega_1)Y_2^n(\Omega_0)\right\rangle_p \\
&\quad + 2\lambda_2^2\frac{(1+2a_x)(1-a_x)}{3}\frac{4}{3}\sqrt{\frac{\pi}{5}}\sum_m\left\langle E^2(t)\left(E^2(0)-\langle E^2\rangle\right)D^2_{m0}(\alpha_1,\beta_1,\gamma_1)\right\rangle\left\langle Y_2^m(\Omega_1)\right\rangle_p,
\end{aligned}
\tag{A10}
$$

where the averages of statistically independent quantities were factored in the final equality. The final term contains averages including the field frame orientation, $(\alpha_1,\beta_1,\gamma_1)$, and molecular frame orientation, Ω_1, at a single time point, t. In an isotropic medium, there are no special orientations, so this term (i.e., the summation as a whole) vanishes. The scalar term (first line in the final equality) is in its simplest form. The correlation function of squared electric field magnitudes decays to $\langle E^2\rangle^2$ at long times, so the scalar term decays to zero. To further simplify the vector term (second term in final equality), we use the orthogonality condition,

$$
\left\langle A_1A_0D^l_{m,n}(\alpha_1,\beta_1,\gamma_1)D^k_{m',n'}(\alpha_0,\beta_0,\gamma_0)\right\rangle \propto \delta_{m,-m'}\delta_{n,-n'},
\tag{A11}
$$

with A_1 and A_0 scalar functions evaluated at the same (time) points as the Euler angles indexed by 1 and 0, respectively.[32] With Eq. (A11) and standard relations for Wigner rotation matrices and spherical harmonics,[78] Equation (A10) becomes,

$$
\begin{aligned}
C_p(t) &= \lambda_2^2\left(\frac{1+2a_x}{3}\right)^2 \left(\left\langle E^2(t)E^2(0)\right\rangle - \langle E^2\rangle^2\right) \\
&\quad + \lambda_2^2(1-a_x)^2\frac{16\pi}{45}\sum_m\left\langle E^2(t)E^2(0)D^2_{m0}(\alpha_1,\beta_1,\gamma_1){D^2_{m0}}^*(\alpha_0,\beta_0,\gamma_0)\right\rangle\left\langle Y_2^m(\Omega_1)Y_2^{m*}(\Omega_0)\right\rangle_p.
\end{aligned}
\tag{A12}
$$

As mentioned above, every axis system is equivalent in an isotropic medium. The isotropic correlation function including the field frame orientation in Eq. (A12) should therefore be independent of the m-index in the rotation matrices.[84] We define the vector correlation function of the field squared as,

$$
H(t) = \left\langle E^2(t)E^2(0)D^2_{m0}(\alpha_1,\beta_1,\gamma_1){D^2_{m0}}^*(\alpha_0,\beta_0,\gamma_0)\right\rangle,
\tag{A13}
$$

and factor $H(t)$ out of the sum in Eq. (A12) to obtain,

$$
\begin{aligned}
C_p(t) &= \lambda_2^2\left(\frac{1+2a_x}{3}\right)^2 \left(\left\langle E^2(t)E^2(0)\right\rangle - \langle E^2\rangle^2\right) \\
&\quad + \lambda_2^2(1-a_x)^2\,H(t)\frac{16\pi}{45}\sum_m\left\langle Y_2^m(\Omega_1)Y_2^{m*}(\Omega_0)\right\rangle_p.
\end{aligned}
\tag{A14}
$$

In $H(t)$, the m values can be 2, 1, 0, −1, or −2. Like an atomic d orbital, for which the energy (a scalar) depends on l but not m, isotropic quantities involving D^2_{m0} do not depend on the value of m.

To evaluate the sum of polarization weighted correlation functions of spherical harmonics appearing in (A14), the probability evolution Green's function for the orientation of the molecular probe is expanded as a sum over all products of spherical harmonics,

$$
G(\Omega_1,t\,|\Omega_0) = \sum_{l=0}^{\infty}\sum_{m=-l}^{l} c_l^m(t)Y_l^m(\Omega_1)Y_l^{m*}(\Omega_0).
$$

The expansion coefficients are,

$$
c_l^m(t) = C_l(t) = \langle P_l(\hat{\mu}(t)\cdot\mu(0))\rangle,
\tag{A15}
$$

the lth order Legendre polynomial orientational correlation functions of the transition dipole unit vector $\hat{\mu}$.[33,79,85] With the Green's function and transition dipole–laser field overlap

factors[79,86] written in terms of spherical harmonics, the integrations over initial and final orientations necessary for evaluation of the polarization-weighted average in Eq. (A14) are straightforward to perform analytically.[33,78] Using the same analytical computation methods as detailed previously for the first order Stark effect PW-FFCFs,[33] we calculate the averages in Eq. (A14) for the $\langle XXXX\rangle$ (polarization of the first two pulses parallel to the third pulse and echo pulse), $\langle XXYY\rangle$ (polarization of the first two pulses perpendicular to the third pulse and echo pulse), and isotropic (the first two pulses at the magic angle to the third pulse and the echo, isotropically averaged) polarization configurations. It is important to note that the isotropically averaged configuration does not eliminate RISD contribution from the observed dynamics. We first write,

$$\sum_m \left\langle Y_2^m(\Omega_1)Y_2^{m*}(\Omega_0)\right\rangle_p = \frac{5}{4\pi}R_p^{(2)}(t), \tag{A16}$$

where $R_p^{(l)}(t)$ in general is the normalized, polarization-weighted, spherical harmonic correlation function sum for order l (discussed below). The particular results of evaluating $R_p^{(2)}(t)$ are,

$$R^{(2)}_{\text{parallel}}(t) = \frac{1}{175}\left[\frac{28 + 215C_2(t) + 72C_4(t)}{1 + 4/5C_2(t)}\right], \tag{A17a}$$

for the $\langle XXXX\rangle$ configuration,

$$R^{(2)}_{\text{perpendicular}}(t) = \frac{1}{175}\left[\frac{-14 + 155C_2(t) - 36C_4(t)}{1 - 2/5C_2(t)}\right], \tag{A17b}$$

for the $\langle XXYY\rangle$ configuration, and

$$R^{(2)}_{\text{isotropic}}(t) = C_2(t), \tag{A17c}$$

for the overall isotropic average or magic angle configuration.

Some comments are warranted on the general form of RISD factors such as those in Eqs. (A17). In third-order nonlinear optical experiments (such as 2D IR), which involve four field-matter interactions, $C_2(t)$ can always appear in the normalization constant for the weighting factors in a polarization-weighted average.[33] Hence, the second order orientational correlation function can appear in the denominator of any RISD factor. Beyond this, consider the correlation functions of spherical harmonics of order l with (un-normalized) transition dipole–laser field overlap factors. It is not difficult to show, using the selection rules for integrals of spherical harmonics,[78] that only orientational correlation functions of order l, $l + 2$, and $|l - 2|$ can appear in general.

The normalized $R_p^{(2)}$ functions above, calculated for particular polarizations p, appeared naturally in the evaluation of Eqs. (A14) and (A16). In general, such normalized, polarization-selectively averaged RISD functions can be defined for any order $l > 0$. The interpretation of the $R_p^{(l)}$ functions is straightforward: if a system's frequency fluctuation is given by $\delta\omega^{(l)}(t) = \Delta \times Y_l^0(\Omega_F(t))$ (angle expressed in the sample field frame, with Δ the characteristic fluctuation amplitude) and *all changes in* Ω_F *are due to molecular reorientation*, then it can be shown that the PW-FFCF is,

$$\langle \delta\omega^{(l)}(t)\delta\omega^{(l)}(0)\rangle_p = \frac{\Delta^2}{4\pi}R_p^{(l)}(t), \tag{A18}$$

using the orthonormality property of the spherical harmonics. We have made the general definition,

$$R_p^{(l)}(t) = \frac{\sum\limits_m \left\langle Y_l^m(\Omega_1)Y_l^{m*}(\Omega_0)\right\rangle_p}{\sum\limits_m \left\langle \left|Y_l^m(\Omega_1)\right|^2\right\rangle_p}, \tag{A19}$$

with angles written in the lab frame, and identify Eq. (A16) as a special case of (A19). For this class of models, all spectral diffusion is due to RISD from the orientational motion of the probe.[33] The normalized results from Eqs. (A18) and (A19) appear as multiplicative factors in more complete models of the FFCF that include structural spectral diffusion (e.g., time variation of Δ).[32]

The normalized polarization-dependent decay functions for $l = 2$, which appeared in Eqs. (A16) and (A18), are presented in Figure 8 for the three cases in Eqs. (A17) using a purely diffusive reorientation model and no structural spectral diffusion (see Section IV). The $R_p^{(1)}(t)$ factors for the same polarization configurations as in Eqs. (A17), using a first order Stark model (Y_1^0 potential in Eq. (A18)), have been reported previously.[32,33] The decay time constants for the first order Stark effect are approximately a factor of 3 times longer than those presented here for the Y_2^0 potential in Eqs. (A17) and Figure 8.

We return now to the full second order Stark model, with both RISD and SSD, which resulted in Eq. (A14). Substitution of the key intermediate result, Eq. (A16) with Eqs. (A17), gives the complete expression for the PW-FFCF,

$$C_p(t) = \lambda_2^2\left(\frac{1 + 2a_x}{3}\right)^2\left(\langle E^2(t)E^2(0)\rangle - \langle E^2\rangle^2\right) + \frac{4\lambda_2^2(1 - a_x)^2}{9}H(t)R_p^{(2)}(t), \tag{A20}$$

with the $H(t)$ vector field-squared correlation function defined in Eq. (A13). In the full correlation function, the normalized RISD functions discussed above are modified by the $H(t)$ factor to decay more quickly due to the fluctuations of the sample's electric field caused by SSD. Added to this term is the scalar correlation function of the field squared, with its long-time offset subtracted. If the vibrational transition dipole is fixed in space (no molecular reorientation), the $R_p^{(2)}$ factor is fixed at unity and the result is simply the sum of both correlation functions of the electric field squared.

In the analysis of experimental spectral diffusion data, such as the decay of the CLS,[63,64] the quantities λ_2, a_x, the initial values of the scalar and vector field squared correlation functions in Eq. (A20) are generally unknown. For the restrictive assumptions of complete independence of electric field orientation and magnitude, as well as Gaussian fluctuation dynamics of the magnitudes, the initial values of the two structural correlation functions can be determined, and they can both be written in terms of the field magnitude correlation function $\langle E(t)E(0)\rangle$ and the second Legendre polynomial orientational correlation function of the field unit vector. In this case, both a_x and $\lambda_2^2\langle E^2\rangle^2$, in

principle, can be determined from the data. Additionally, spectral diffusion in systems with both first and second order Stark effects could be analyzed with relatively few free parameters, allowing determination of the relative Stark coupling constants. However, the decoupling of a liquid or other sample's electric field orientation and magnitude is unlikely to hold in practice.

The restrictive assumptions above that simplify the PW-FFCF do not apply for the experimental investigation presented here. In general, we can write the polarization-weighted frequency-frequency correlation function in Eq. (A20) in the most condensed form as,

$$C_p(t) = \langle \delta\omega(t)\delta\omega(0)\rangle_p = F_s(t) + F_v(t)R_p^{(2)}(t). \quad \text{(A21)}$$

The $R_p^{(2)}(t)$ factors are given in Equations (A17). Here, $F_s(t)$ and $F_v(t)$ (Eqs. (10) and (11) in the main text) are the correlation functions for the structural dynamics for vibrational probes that are scalar and vector coupled to the medium electric field, respectively. Sums of exponentials have been used extensively as models of FFCFs and are appropriate for these structural correlation functions.

[1]T. Gasser, C. Guivarch, K. Tachiiri, C. D. Jones, and P. Ciais, "Negative emissions physically needed to keep global warming below 2°C," Nat. Commun. **6**, 7958 (2015).

[2]R. S. Haszeldine, "Carbon capture and storage: How green can black be?," Science **325**(5948), 1647–1652 (2009).

[3]A. H. Lu and S. Dai, *Porous Materials for Carbon Dioxide Capture* (Springer, Berlin, Heidelberg, 2014).

[4]M. E. Boot-Handford, J. C. Abanades, E. J. Anthony, M. J. Blunt, S. Brandani, N. Mac Dowell, J. R. Fernandez, M.-C. Ferrari, R. Gross, J. P. Hallett, R. S. Haszeldine, P. Heptonstall, A. Lyngfelt, Z. Makuch, E. Mangano, R. T. J. Porter, M. Pourkashanian, G. T. Rochelle, N. Shah, J. G. Yao, and P. S. Fennell, "Carbon capture and storage update," Energy Environ. Sci. **7**(1), 130–189 (2014).

[5]J. D. Figueroa, T. Fout, S. Plasynski, H. McIlvried, and R. D. Srivastava, "Advances in CO_2 capture technology—The U.S. Department of Energy's Carbon Sequestration Program," Int. J. Greenhouse Gas Control **2**(1), 9–20 (2008).

[6]T. C. Merkel, H. Lin, X. Wei, and R. Baker, "Power plant post-combustion carbon dioxide capture: An opportunity for membranes," J. Membr. Sci. **359**(1-2), 126–139 (2010).

[7]U. S. Energy Information Administration, "Electric Power Annual 2013," U. S. Department of Energy, Washington, DC, 2015.

[8]R. Hayes, G. G. Warr, and R. Atkin, "Structure and nanostructure in ionic liquids," Chem. Rev. **115**(13), 6357–6426 (2015).

[9]N. V. Plechkova and K. R. Seddon, "Applications of ionic liquids in the chemical industry," Chem. Soc. Rev. **37**, 123–150 (2008).

[10]J. P. Hallett and T. Welton, "Room-temperature ionic liquids: Solvents for synthesis and catalysis. 2," Chem. Rev. **111**(5), 3508–3576 (2011).

[11]T. Welton, "Room-temperature ionic liquids. Solvents for synthesis and catalysis," Chem. Rev. **99**(8), 2071–2084 (1999).

[12]E. Torralba-Calleja, J. Skinner, and D. Gutirrez-Tauste, "CO_2 capture in ionic liquids: A review of solubilities and experimental methods," J. Chem. **2013**, 16.

[13]R. Condemarin and P. Scovazzo, "Gas permeabilities, solubilities, diffusivities, and diffusivity correlations for ammonium-based room temperature ionic liquids with comparison to imidazolium and phosphonium RTIL data," Chem. Eng. J. **147**(1), 51–57 (2009).

[14]M. S. Shannon and J. E. Bara, "Properties of alkylimidazoles as solvents for CO_2 capture and comparisons to imidazolium-based ionic liquids," Ind. Eng. Chem. Res. **50**(14), 8665–8677 (2011).

[15]E. D. Bates, R. D. Mayton, I. Ntai, and J. H. Davis, "CO_2 capture by a task-specific ionic liquid," J. Am. Chem. Soc. **124**(6), 926–927 (2002).

[16]J. E. Bara, D. E. Camper, D. L. Gin, and R. D. Noble, "Room-temperature ionic liquids and composite materials: Platform technologies for CO_2 capture," Acc. Chem. Res. **43**(1), 152–159 (2010).

[17]X. Zhang, X. Zhang, H. Dong, Z. Zhao, S. Zhang, and Y. Huang, "Carbon capture with ionic liquids: Overview and progress," Energy Environ. Sci. **5**(5), 6668–6681 (2012).

[18]M. Ramdin, T. W. de Loos, and T. J. H. Vlugt, "State-of-the-art of CO_2 capture with ionic liquids," Ind. Eng. Chem. Res. **51**(24), 8149–8177 (2012).

[19]C. Cadena, J. L. Anthony, J. K. Shah, T. I. Morrow, J. F. Brennecke, and E. J. Maginn, "Why is CO_2 so soluble in imidazolium-based ionic liquids?," J. Am. Chem. Soc. **126**(16), 5300–5308 (2004).

[20]M. Armand, F. Endres, D. R. MacFarlane, H. Ohno, and B. Scrosati, "Ionic-liquid materials for the electrochemical challenges of the future," Nat. Mater. **8**(8), 621–629 (2009).

[21]H. Shirota, T. Mandai, H. Fukazawa, and T. Kato, "Comparison between dicationic and monocationic ionic liquids: Liquid density, thermal properties, surface tension, and shear viscosity," J. Chem. Eng. Data **56**(5), 2453–2459 (2011).

[22]A. Yokozeki, M. B. Shiflett, C. P. Junk, L. M. Grieco, and T. Foo, "Physical and chemical absorptions of carbon dioxide in room-temperature ionic liquids," J. Phys. Chem. B **112**(51), 16654–16663 (2008).

[23]S. S. Moganty and R. E. Baltus, "Diffusivity of carbon dioxide in room-temperature ionic liquids," Ind. Eng. Chem. Res. **49**(19), 9370–9376 (2010).

[24]T. Umecky, M. Kanakubo, T. Makino, T. Aizawa, and A. Suzuki, "Effect of CO_2 dissolution on electrical conductivity and self-diffusion coefficients of 1-butyl-3-methylimidazolium hexafluorophosphate ionic liquid," Fluid Phase Equilib. **357**, 76–79 (2013).

[25]Y. Hou and R. E. Baltus, "Experimental measurement of the solubility and diffusivity of CO_2 in room-temperature ionic liquids using a transient thin-liquid-film method," Ind. Eng. Chem. Res. **46**(24), 8166–8175 (2007).

[26]D. Camper, C. Becker, C. Koval, and R. Noble, "Diffusion and solubility measurements in room temperature ionic liquids," Ind. Eng. Chem. Res. **45**(1), 445–450 (2006).

[27]K. Kortenbruck, B. Pohrer, E. Schluecker, F. Friedel, and I. Ivanovic-Burmazovic, "Determination of the diffusion coefficient of CO_2 in the ionic liquid EMIM NTf_2 using online FTIR measurements," J. Chem. Thermodyn. **47**, 76–80 (2012).

[28]D. Morgan, L. Ferguson, and P. Scovazzo, "Diffusivities of gases in room-temperature ionic liquids: Data and correlations obtained using a lag-time technique," Ind. Eng. Chem. Res. **44**(13), 4815–4823 (2005).

[29]C. Moya, J. Palomar, M. Gonzalez-Miquel, J. Bedia, and F. Rodriguez, "Diffusion coefficients of CO_2 in ionic liquids estimated by gravimetry," Ind. Eng. Chem. Res. **53**(35), 13782–13789 (2014).

[30]E. D. Hazelbaker, S. Budhathoki, A. Katihar, J. K. Shah, E. J. Maginn, and S. Vasenkov, "Combined application of high-field diffusion NMR and molecular dynamics simulations to study dynamics in a mixture of carbon dioxide and an imidazolium-based ionic liquid," J. Phys. Chem. B **116**(30), 9141–9151 (2012).

[31]T. Brinzer, E. J. Berquist, Z. Ren, S. Dutta, C. A. Johnson, C. S. Krisher, D. S. Lambrecht, and S. Garrett-Roe, "Ultrafast vibrational spectroscopy (2D-IR) of CO_2 in ionic liquids: Carbon capture from carbon dioxide's point of view," J. Chem. Phys. **142**(21), 212425 (2015).

[32]P. L. Kramer, J. Nishida, and M. D. Fayer, "Separation of experimental 2D IR frequency-frequency correlation functions into structural and reorientation-induced contributions," J. Chem. Phys. **143**(12), 124505 (2015).

[33]P. L. Kramer, J. Nishida, C. H. Giammanco, A. Tamimi, and M. D. Fayer, "Observation and theory of reorientation-induced spectral diffusion in polarization-selective 2D IR spectroscopy," J. Chem. Phys. **142**(18), 184505 (2015).

[34]K. Kinosita, A. Ikegami, and S. Kawato, "On the wobbling-in-cone analysis of fluorescence anisotropy decay," Biophys. J. **37**(2), 461–464 (1982).

[35]K. Kinosita, S. Kawato, and A. Ikegami, "Theory of fluorescence polarization decay in membranes," Biophys. J. **20**, 289–305 (1977).

[36]P. L. Kramer, C. H. Giammanco, and M. D. Fayer, "Dynamics of water, methanol, and ethanol in a room temperature ionic liquid," J. Chem. Phys. **142**(21), 212408 (2015).

[37]G. Lipari and A. Szabo, "Effect of librational motion on fluorescence depolarization and nuclear magnetic-resonance relaxation in macromolecules and membranes," Biophys. J. **30**(3), 489–506 (1980).

[38]H.-S. Tan, I. R. Piletic, and M. D. Fayer, "Orientational dynamics of water confined on a nanometer length scale in reverse micelles," J. Chem. Phys. **122**, 174501 (2005).

[39]C. C. Wang and R. Pecora, "Time-correlation functions for restricted rotational diffusion," J. Chem. Phys. **72**(10), 5333–5340 (1980).

[40]P. G. Maiella, J. W. Schoppelrei, and T. B. Brill, "Spectroscopy of hydrothermal reactions. Part XI: Infrared absorptivity of CO_2 and N_2O in water at elevated temperature and pressure," Appl. Spectrosc. **53**(3), 351–355 (1999).

[41]G. Moore, A. Chizmeshya, and P. F. McMillan, "Calibration of a reflectance FTIR method for determination of dissolved CO_2 concentration in rhyolitic glasses," Geochim. Cosmochim. Acta **64**(20), 3571–3579 (2000).
[42]E. E. Fenn, D. B. Wong, and M. D. Fayer, "Water dynamics in small reverse micelles in two solvents: Two-dimensional infrared vibrational echoes with two-dimensional background subtraction," J. Chem. Phys. **134**, 054512 (2011).
[43]S. K. Karthick Kumar, A. Tamimi, and M. D. Fayer, "Comparisons of 2D IR measured spectral diffusion in rotating frames using pulse shaping and in the stationary frame using the standard method," J. Chem. Phys. **137**(18), 184201 (2012).
[44]S. Park, K. Kwak, and M. D. Fayer, "Ultrafast 2D-IR vibrational echo spectroscopy: A probe of molecular dynamics," Laser Phys. Lett. **4**, 704–718 (2007).
[45]S. M. Gallagher Faeder and D. M. Jonas, "Two-dimensional electronic correlation and relaxation spectra: Theory and model calculations," J. Phys. Chem. A **103**(49), 10489–10505 (1999).
[46]S.-H. Shim, D. B. Strasfeld, E. C. Fulmer, and M. T. Zanni, "Femtosecond pulse shaping directly in the mid-IR using acousto-optic modulation," Opt. Lett. **31**(6), 838–840 (2006).
[47]S.-H. Shim and M. T. Zanni, "How to turn your pump-probe instrument into a multidimensional spectrometer: 2D IR and vis spectroscopiesvia pulse shaping," Phys. Chem. Chem. Phys. **11**(5), 748–761 (2009).
[48]S. Garrett-Roe and P. Hamm, "Purely absorptive three-dimensional infrared spectroscopy," J. Chem. Phys. **130**(16), 164510 (2009).
[49]T. Seki, J.-D. Grunwaldt, and A. Baiker, "*In situ* attenuated total reflection infrared spectroscopy of imidazolium-based room-temperature ionic liquids under 'supercritical' CO_2," J. Phys. Chem. B **113**(1), 114–122 (2009).
[50]J. J. Potoff and J. I. Siepmann, "Vapor–liquid equilibria of mixtures containing alkanes, carbon dioxide, and nitrogen," AIChE J. **47**(7), 1676–1682 (2001).
[51]X. Huang, C. J. Margulis, Y. Li, and B. J. Berne, "Why is the partial molar volume of CO_2 so small when dissolved in a room temperature ionic liquid? Structure and dynamics of CO_2 dissolved in [Bmim$^+$] [PF$_6^-$]," J. Am. Chem. Soc. **127**(50), 17842–17851 (2005).
[52]D. B. Wong, C. H. Giammanco, E. E. Fenn, and M. D. Fayer, "Dynamics of isolated water molecules in a sea of ions in a room temperature ionic liquid," J. Phys. Chem. B **117**, 623–635 (2012).
[53]L. Cammarata, S. G. Kazarian, P. A. Salter, and T. Welton, "Molecular states of water in room temperature ionic liquids," Phys. Chem. Chem. Phys. **3**, 5192–5200 (2001).
[54]C. H. Giammanco, P. L. Kramer, S. A. Yamada, J. Nishida, A. Tamimi, and M. D. Fayer, "Coupling of carbon dioxide stretch and bend vibrations reveals thermal population dynamics in an ionic liquid," J. Phys. Chem. B **120**, 549 (2016).
[55]D. E. Moilanen, E. E. Fenn, Y. S. Lin, J. L. Skinner, B. Bagchi, and M. D. Fayer, "Water inertial reorientation: Hydrogen bond strength and the angular potential," Proc. Natl. Acad. Sci. U. S. A. **105**(14), 5295–5300 (2008).
[56]R. S. Moog, M. D. Ediger, S. G. Boxer, and M. D. Fayer, "Viscosity dependence of the rotational reorientation of rhodamine B in mono- and polyalcohol. Picosecond transient grating experiments," J. Phys. Chem. **86**, 4694–4700 (1982).
[57]G. K. Youngren and A. Acrivos, "Rotational friction coefficients for ellipsoids and chemical molecules with the slip boundary condition," J. Chem. Phys. **63**, 3846–3849 (1975).
[58]C.-M. Hu and R. Zwanzig, "Rotational friction coefficients for spheroids with the slipping boundary condition," J. Chem. Phys. **60**, 4354–4357 (1974).
[59]L. Pauling, *The Nature of the Chemical Bond and the Structure of Molecules and Crystals: An Introduction to Modern Structural Chemistry* (Cornell University Press, 1960).
[60]A. Kaintz, G. Baker, A. Benesi, and M. Maroncelli, "Solute diffusion in ionic liquids, NMR measurements and comparisons to conventional solvents," J. Phys. Chem. B **117**(39), 11697–11708 (2013).
[61]J. C. Araque, S. K. Yadav, M. Shadeck, M. Maroncelli, and C. J. Margulis, "How is diffusion of neutral and charged tracers related to the structure and dynamics of a room-temperature ionic liquid? Large deviations from Stokes–Einstein behavior explained," J. Phys. Chem. B **119**(23), 7015–7029 (2015).
[62]P. Hamm and M. T. Zanni, *Concepts and Methods of 2D Infrared Spectroscopy* (Cambridge University Press, Cambridge, New York, 2011).
[63]K. Kwak, S. Park, I. J. Finkelstein, and M. D. Fayer, "Frequency-frequency correlation functions and apodization in 2D-IR vibrational echo spectroscopy, a new approach," J. Chem. Phys. **127**, 124503 (2007).
[64]K. Kwak, D. E. Rosenfeld, and M. D. Fayer, "Taking apart the two-dimensional infrared vibrational echo spectra: More information and elimination of distortions," J. Chem. Phys. **128**(20), 204505 (2008).
[65]A. Tamimi and M.D. Fayer, "Ionic liquid dynamics measured with 2D IR and IR pump–probe experiments on a linear anion and the influence of potassium cations," J. Phys. Chem. B, Article ASAP (published online 2016).
[66]S. Mukamel, *Principles of Nonlinear Optical Spectroscopy* (Oxford University Press, New York, 1995).
[67]R. B. Williams, R. F. Loring, and M. D. Fayer, "Vibrational dephasing of carbonmonoxy myoglobin," J. Phys. Chem. B **105**, 4068–4071 (2001).
[68]P. L. Geissler, "Water interfaces, solvation, and spectroscopy," Annu. Rev. Phys. Chem. **64**(1), 317–337 (2013).
[69]S. Bagchi, S. G. Boxer, and M. D. Fayer, "Ribonuclease S dynamics measured using a nitrile label with 2D IR vibrational echo spectroscopy," J. Phys. Chem. B **116**, 4034–4042 (2012).
[70]S. D. Fried, S. Bagchi, and S. G. Boxer, "Measuring electrostatic fields in both hydrogen-bonding and non-hydrogen-bonding environments using carbonyl vibrational probes," J. Am. Chem. Soc. **135**(30), 11181–11192 (2013).
[71]Z. L. Terranova and S. A. Corcelli, "Molecular dynamics investigation of the vibrational spectroscopy of isolated water in an ionic liquid," J. Phys. Chem. B **118**(28), 8264–8272 (2014).
[72]S. Corcelli and J. L. Skinner, "Infrared and Raman line shapes of dilute HOD in liquid H_2O and D_2O from 10 to 90 °C," J. Phys. Chem. A **109**, 6154–6165 (2005).
[73]S. Corcelli, C. P. Lawrence, and J. L. Skinner, "Combined electronic structure/molecular dynamics approach for ultrafast infrared spectroscopy of dilute HOD in liquid H_2O and D_2O," J. Chem. Phys. **120**, 8107–8117 (2004).
[74]C. P. Lawrence and J. L. Skinner, "Vibrational spectroscopy of HOD in liquid D_2O. III. Spectral diffusion, and hydrogen-bonding and rotational dynamics," J. Chem. Phys. **118**, 264–272 (2003).
[75]G. U. Bublitz and S. G. Boxer, "Stark spectroscopy: Applications in chemistry, biology, and materials science," Annu. Rev. Phys. Chem. **48**(1), 213–242 (1997).
[76]S. G. Boxer, "Stark realities," J. Phys. Chem. B **113**(10), 2972–2983 (2009).
[77]S. S. Andrews and S. G. Boxer, "Vibrational Stark effects of nitriles I. Methods and experimental results," J. Phys. Chem. A **104**(51), 11853–11863 (2000).
[78]R. N. Zare, *Angular Momentum* (Wiley-Interscience, 1988).
[79]A. Tokmakoff, "Orientational correlation functions and polarization selectivity for nonlinear spectroscopy of isotropic media. I. Third order," J. Chem. Phys. **105**(1), 1–12 (1996).
[80]K. P. Sokolowsky, H. E. Bailey, and M. D. Fayer, "New divergent dynamics in the isotropic to nematic phase transition of liquid crystals measured with 2D IR vibrational echo spectroscopy," J. Chem. Phys. **141**(19), 194502 (2014).
[81]A. L. Sturlaugson, A. Y. Arima, H. E. Bailey, and M. D. Fayer, "Orientational dynamics in a lyotropic room temperature ionic liquid," J. Phys. Chem. B **117**, 14775–14784 (2013).
[82]S. S. Andrews, Ph.D. thesis, Stanford University, 2001.
[83]I. J. Finkelstein, A. Goj, B. L. McClain, A. M. Massari, K. A. Merchant, R. F. Loring, and M. D. Fayer, "Ultrafast dynamics of myoglobin without the distal histidine: Stimulated vibrational echo experiments and molecular dynamics simulations," J. Phys. Chem. B **109**(35), 16959–16966 (2005).
[84]B. J. Berne and R. Pecora, *Dynamic Light Scattering* (Dover, Mineola, New York, 2000).
[85]T. Tao, "Time-dependent fluorescence depolarization and Brownian rotational diffusion coefficients of macromolecules," Biopolymers **8**, 609–632 (1969).
[86]J. Nishida and M. D. Fayer, "Theory of third-order spectroscopic methods to extract detailed molecular orientational dynamics for planar surfaces and other uniaxial systems," J. Chem. Phys. **140**(14), 144702 (2014).